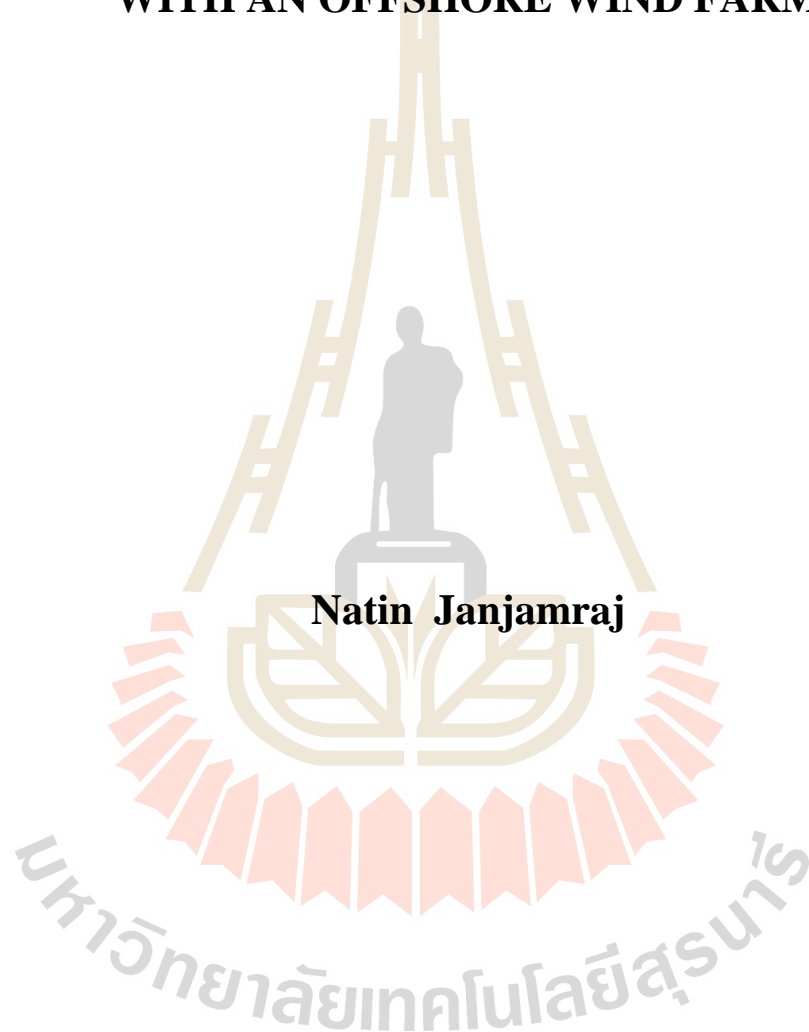


**A STUDY OF MODULAR MULTILEVEL CONVERTER
IMPROVEMENT ON POWER SYSTEM INTEGRATED
WITH AN OFFSHORE WIND FARM**



Natin Janjamraj

A Thesis Submitted in Partial Fulfillment of the Requirements for the

Degree of Doctor of Philosophy in Electrical Engineering

Suranaree University of Technology

Academic Year 2016

การปรับปรุงมอดูลาร์มัลติเลเวลคอนเวอร์เตอร์ของระบบไฟฟ้ากำลังที่
ประกอบด้วยทุ่งกัณฑ์นลมนอกชายฝั่ง



นายณตฤณ จันท์จรัส

วิทยานิพนธ์นี้เป็นส่วนหนึ่งของการศึกษาตามหลักสูตรปริญญาวิศวกรรมศาสตรดุษฎีบัณฑิต

สาขาวิชาวิศวกรรมไฟฟ้า


มหาวิทยาลัยเทคโนโลยีสุรนารี

ปีการศึกษา 2559

**A STUDY OF MODULAR MULTILEVEL CONVERTER
IMPROVEMENT ON POWER SYSTEM INTEGRATED WITH AN
OFFSHORE WIND FARM**


Suranaree University of Technology has approved this thesis submitted in partial fulfillment of the requirements for the Degree of Doctor of Philosophy.

Thesis Examining Committee



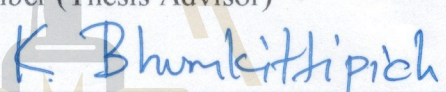
(Assoc. Prof. Dr. Thanatchai Kulworawanichpong)

Chairperson




(Assoc. Prof. Dr. Anant Oonsivilai)

Member (Thesis Advisor)




(Assoc. Prof. Dr. Krischonme Bhumkittipich)

Member



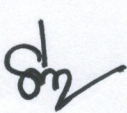
(Asst. Prof. Dr. Boonruang Marungsri)

Member



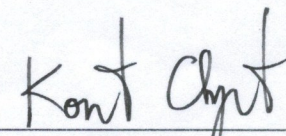
(Asst. Prof. Dr. Padej Pao-la-or)

Member



(Prof. Dr. Santi Maensiri)

Vice Rector for Academic Affairs
and Internationalization



(Assoc. Prof. Flt. Lt. Dr. Kontorn Chamniprasart)

Dean of Institute of Engineering

ณตฤณ จันทร์จรัส : การปรับปรุงมอดูลาร์มัลติเลเวลคอนเวอร์เตอร์ของระบบไฟฟ้ากำลังที่ประกอบด้วยทุ้งกังหันลมนอกชายฝั่ง (A STUDY OF MODULAR MULTILEVEL CONVERTER IMPROVEMENT ON POWER SYSTEM INTEGRATED WITH AN OFFSHORE WIND FARM) อาจารย์ที่ปรึกษา : รองศาสตราจารย์ ดร.อนันต์ อุ่นศิริไธย์, 185 หน้า.

วัตถุประสงค์ของการวิจัยนี้เป็นการปรับปรุงระบบไฟฟ้ากระแสตรงแรงดันสูงที่ใช้มอดูลาร์มัลติเลเวลคอนเวอร์เตอร์ โดยได้ศึกษาวิจัยเพื่อปรับปรุงทั้งสมรรถนะของคอนเวอร์เตอร์และสมรรถนะของระบบควบคุม ในการปรับปรุงสมรรถนะของคอนเวอร์เตอร์ การศึกษาวิจัยนี้ได้ปรับปรุงความเพี้ยนเชิงฮาร์มอนิกรวมของแรงดันด้านออกโดยใช้วิธีการหาค่าที่เหมาะสมที่สุดแบบกลุ่มอนุภาคเพื่อออกแบบหาค่ามุมในการมอดูเลตมอดูลาร์มัลติเลเวลคอนเวอร์เตอร์เพื่อให้ได้ค่าความเพี้ยนเชิงฮาร์มอนิกรวมต่ำที่สุด และสำหรับการปรับปรุงระบบควบคุมระบบไฟฟ้ากระแสตรงแรงดันสูงชนิดใช้มอดูลาร์มัลติเลเวลคอนเวอร์เตอร์ที่เชื่อมต่อกับทุ้งกังหันลมนอกชายฝั่งกับระบบไฟฟ้ากำลังนั้น งานวิจัยนี้ได้ปรับปรุงตัวแปรในตัวควบคุมแบบ PI ของระบบ

สมรรถนะที่สำคัญอย่างหนึ่งของคอนเวอร์เตอร์ชนิดแหล่งจ่ายแรงดันคือฮาร์มอนิกของแรงดันด้านออกที่จะจ่ายให้กับระบบไฟฟ้า ดังนั้นงานวิจัยนี้จึงได้นำเสนอวิธีการหาค่าที่เหมาะสมที่สุดแบบกลุ่มอนุภาคในการค้นหาค่ามุมในการสั่งให้อุปกรณ์อิเล็กทรอนิกส์กำลังทำงานที่เหมาะสมเพื่อใช้ในการมอดูเลตคอนเวอร์เตอร์ และศึกษาเปรียบเทียบกับมอดูเลตโดยวิธีพีดับปลิวเอ๋มที่นิยมใช้ทั่วไป โดยได้ทำการศึกษาและวิเคราะห์เปรียบเทียบมอดูลาร์มัลติเลเวลคอนเวอร์เตอร์ทั้งสองชนิดที่มีจำนวนระดับ 3, 9, 11, 15, 27, 73 และ 101 ระดับ ผลการศึกษาพบว่าค่าความเพี้ยนเชิงฮาร์มอนิกรวมโดยวิธีหาค่าที่เหมาะสมที่สุดที่นำเสนอให้ผลที่ดีกว่าการมอดูเลตโดยวิธีพีดับปลิวเอ๋มทุก ๆ การศึกษาเปรียบเทียบกันที่จำนวนระดับของคอนเวอร์เตอร์เท่ากัน โดยมีค่าดีกว่าเฉลี่ยประมาณ 12.7%

สำหรับสมรรถนะของระบบควบคุมสามารถประเมินบนพื้นฐานของพฤติกรรม การตอบสนองพลวัต ระบบการควบคุม VSC-HVDC ที่ต่อระหว่างทุ้งกังหันลมนอกชายฝั่งกับระบบไฟฟ้ากำลังโดยใช้ตัวควบคุมแบบ PI ในการปรับปรุงการตอบสนองพลวัตนี้ทำโดยการปรับค่าตัวแปร K_i และ K_p ของตัวควบคุมแบบ PI การวิจัยนี้ได้ทดสอบค่าความคลาดเคลื่อนของแรงดันด้านออกโดยใช้ทฤษฎีของ Ziegler และ Nichols, IAE, ISE, IATE และ ITSE และปรับปรุงสมรรถนะการตอบสนองพลวัตของระบบควบคุมโดยใช้ตัวควบคุมแบบ PI และทำการปรับค่าตัวแปรโดยใช้ PSO ผลจากการศึกษาพบว่าสมรรถนะของระบบควบคุมที่ใช้วิธีการค้นหาตัวแปรโดยใช้วิธี PSO+ITAE มีสมรรถนะดีที่สุดคือมีแรงดันพุ่งเกินอยู่ที่ 2.0% ซึ่งดีกว่าวิธีของ Ziegler และ Nichols,

ISE, ITSE, IAE และ ITAE ซึ่งมีค่าแรงดันพุ่งเกินสูงสุด (p_u) อยู่ที่ 27.8%, 19.9%, 13.1%, 9.1% และ 4.4%ตามลำดับ การตอบสนองทางเวลาของวิธี PSO+ITAE สามารถที่จะเข้าสู่สถานะเสถียรภายในเวลา 5.2 วินาที โดยไม่มีแรงดันพุ่งเกิน ยิ่งไปกว่านั้นสมรรถนะอื่นๆ ก็ดีกว่าวิธีเดิมทุกๆ อย่าง โดยมีช่วงเวลาในการหน่วง (t_d) และช่วงเวลาการขึ้นระดับ (t_r) เป็น 1.5 และ 2.6 วินาที ตามลำดับ

ดังนั้นจากการวิจัยนี้แสดงให้เห็นว่าการปรับปรุงทั้งสมรรถนะด้านความเพี้ยนเชิงฮาร์มอนิก รวมของคอนเวอร์เตอร์และสมรรถนะของระบบควบคุมของตัวควบคุมแบบ PI โดยใช้วิธีการหาค่าที่เหมาะสมที่สุดแบบกลุ่มอนุภาคให้ผลที่ดีกว่าการวิธีการเดิมที่นิยมใช้ทั่วไป



สาขาวิชา _____ วิศวกรรมไฟฟ้า _____

ปีการศึกษา 2559

ลายมือชื่อนักศึกษา พ. ภูมิภักดิ์

ลายมือชื่ออาจารย์ที่ปรึกษา CC

NATIN JANJAMRAJ : A STUDY OF MODULAR MULTILEVEL
CONVERTER IMPROVEMENT ON POWER SYSTEM INTEGRATED
WITH AN OFFSHORE WIND FARM. THESIS ADVISOR : ASSOC.
PROF. ANANT OONSIVILAI, Ph.D., 173 PP.

MODULAR MULTILEVEL CONVERTER/ HVDC/ OFFSHORE WIND FARM/
PSO

The objective of this research is both improvements of MMC-based HVDC systems are including the converter performance and controller performance. The converter performance is to improve the total harmonic distortion output waveform and modulation technique of modular multilevel converter (MMC). For control system improvement, this thesis is to improve the PI parameters of MMC-based HVDC transmission systems controllers. The both performances improvement are using artificial intelligence particle swarm optimization (PSO).

The one of most important performance of voltage source converter is output voltage harmonic. Therefore, this research is proposed the particle swarm optimization (PSO) for search the switch angles in modulation and compared with the Carrier-shift SPWM for 3, 9, 11, 15, 27, 73 and 101 levels. The simulation results are shown the voltage THD of PSO method is better than the Carrier-shift SPWM in all and about 12.7% in average.

The performance of the control system is evaluated based on its transient response behavior. The control system of the VSC-HVDC is connected between offshore wind farm and power systems are used the PI controller. For improved the

transient response by adjustment the parameters K_i and K_p of the PI controllers. This research is verified the output voltage errors by Ziegler and Nichols, IAE, ISE, IATE, ITSE and improve the transient performance of control systems by PI controller and tuning its parameters by PSO. The simulation results are shown the parameters are searched by using PSO+ITAE is the best performance by maximum over shoot (P_M) is 2.0% is better than Ziegler and Nichols, ISE, ITSE,IAE and ITAE are 27.8%, 19.9%, 13.1%, 9.1% and 4.4% respectively. The time response of PSO+ITAE method is reach to steady state within 5.2 second without overshoot. Moreover, all performance characteristics are better than the all conventional method with the delay time (t_d) and rise times (t_s) are 1.5 second and 2.6 second respectively.

Therefore, this research is shown both improvements, the THD performance of converters and the control performance of PI controller by using PSO optimization method is effectively than conventional methods.

มหาวิทยาลัยเทคโนโลยีสุรนารี

School of Electrical Engineering

Academic Year 2016

Student's Signature

Advisor's Signature

W. Somde.

CC

ACKNOWLEDGMENTS

The author wishes to acknowledge the funding support of Suranaree University of Technology (SUT).

First, I would like to grateful thanks to Assoc. Prof. Dr. Anant Oonsivilai, thesis advisor, who allowed the author work independently, but gave a critical review of this research.

I would like to thanks are also extended to Assoc. Prof. Dr. Krischonme Bhumkittipich, who served on the thesis committee and commented on the manuscript and thanks the lecturers in the School of Electrical Engineering, Assoc. Prof. Dr. Thanatchai Kulworawanichpong, Asst. Prof. Dr. Boonruang Marungsri and Asst. Prof. Dr. Padej Pao-la-or and many others for suggestions and all their help.

Finally, I am most grateful to my parents and my friends for all their support throughout the period of this research.

Natin Janjamraj

TABLE OF CONTENTS

	Page
ABSTRACT (THAI).....	I
ABSTRACT (ENGLISH).....	III
ACKNOWLEDGEMENTS.....	V
TABLE OF CONTENTS.....	VI
LIST OF TABLES.....	VIII
LIST OF FIGURES.....	XI
CHAPTER	
I INTRODUCTION	1
1.1 Background.....	1
1.2 Motivation.....	2
1.2.1 Wind Farm Applications.....	2
1.2.2 Wind Turbine Application in Thailand.....	6
1.2.3 HVDC Transmission Systems.....	7
1.2.4 Harmonics and Control Systems Performances.....	9
1.3 Research Objectives and Methodologies.....	11
1.4 Scope and Limitation of the Thesis.....	12
1.4.1 Scope of the Thesis.....	12
1.4.2 Limitation of the Thesis.....	13
1.5 Thesis Outline.....	14

TABLE OF CONTENTS (Continued)

	Page
II LITERATURE REVIEW	16
2.1 Introduction.....	16
2.2 Review of HVDC Transmission Systems.....	16
2.3 HVDC Classifications.....	18
2.3.1 Mercury Arc Rectifier Based LCC-HVDC Systems	19
2.3.2 Thyristor Based LCC-HVDC Systems.....	20
2.3.3 CCC-HVDC Systems.....	24
2.3.4 VSC-HVDC Transmission Systems.....	24
2.4 Review of HVDC Configurations.....	25
2.4.1 Back-to-back HVDC Systems.....	25
2.4.2 Point-to-Point HVDC Systems.....	25
2.4.3 Multi-terminal HVDC Systems.....	28
2.5 Review of Control of HVDC Transmission Systems.....	28
2.5.1 Converter Control for HVDC Systems.....	28
2.5.2 Commutation Failure.....	31
2.5.3 Control of HVDC Transmission Systems.....	31
2.6 Conclusions.....	33
III MODELING AND CONTROL OF WIND TURBINES	35

TABLE OF CONTENTS (Continued)

		Page
3.1	Introduction.....	35
3.2	Modeling of DFIG Systems.....	35
3.2.1	Aerodynamic Modeling of Wind Turbine.....	36
3.2.2	Modeling of Two-mass Drive-Train.....	38
3.2.3	Modeling of DFIG.....	40
3.2.4	Modeling of DC Link.....	45
3.3	Control Strategies of DFIG Systems.....	46
3.3.1	The Rotor-Side VSC Controller.....	46
3.3.1	The Grid-Side VSC Controller.....	48
3.4	Modeling of PMSG Systems.....	50
3.4.1	Modeling of Drive-Train.....	53
3.4.2	Modeling of PMSG.....	54
3.4.3	Modeling of DC Link.....	56
3.5	Control Strategies of WT-PMSG Systems.....	56
3.5.1	The Generator-Side VSC Controller.....	57
3.5.2	The Grid-Side VSC Controller.....	59
3.6	Modeling for Offshore Wind Farms.....	60
3.6.1	Assumptions and Simplifications.....	62
3.6.2	Identification of Coherency Groups.....	62
3.6.3	Network Reduction.....	64
3.6.4	Parameter Aggregation of DFIG Systems.....	65

TABLE OF CONTENTS (Continued)

	Page
3.6.4.1 Parameter Aggregation of the Shaft	
Models.....	65
3.6.4.2 Parameter Aggregation of DFIG.....	68
3.6.4.3 Parameter Aggregation of DC Link.....	69
3.6.4.4 Parameter Aggregation of Control	
System.....	69
3.6.5 Parameter Aggregation of PMSG Systems.....	69
3.6.5.1 Parameter Aggregation of the Shaft	
Models.....	69
3.6.5.2 Parameter Aggregation of PMSG	70
3.6.5.3 Parameter Aggregation of DC Link and	
Control System of PMSG.....	70
3.7 Case Studies.....	71
3.7.1 DFIG Connected with Transmission Systems.....	71
3.7.2 PMSG Wind Farm Connected to the Power	
Systems.....	77
3.8 Conclusions.....	81
IV PARTICLE SWARM OPTIMIZED HARMONIC FOR	
MODULAR MULTILEVEL CONVERTER.....	82
4.1 Introduction.....	82
4.2 Modular Multilevel Converter.....	82

TABLE OF CONTENTS (Continued)

	Page
4.3 Optimized Harmonic Stepped Waveform.....	84
4.4 Simulation of OHSW for MMC.....	86
4.5 Simulation Results of OHSW for MMC.....	90
4.6 Harmonic Requirement and Analysis.....	97
4.7 Conclusions.....	98
V MODELING AND CONTROL OF MMC-BASED HVDC	
TRANSMISSION SYSTEMS	99
5.1 Introduction.....	100
5.2 Modeling of VSC-HVDC Transmission System.....	100
5.2.1 Modeling of Rectifier-Side Converter.....	100
5.2.2 Modeling of Inverter-Side Converter.....	104
5.3 Control of Point-to-Point VSC-HVDC System.....	107
5.3.1 The Rectifier-Side VSC-Controller.....	107
5.3.2 The Inverter-Side VSC-Controller.....	110
5.4 Simulation of MMC-Based VSC-HVDC Transmission Systems.....	112
5.4.1 Systems Configurations.....	112
5.4.2 Modulation Techniques.....	116
5.4.2.1 Carrier-Shift SPWM.....	117
5.4.2.2 Optimized Harmonic Stepped Waveform (OHSW).....	118

TABLE OF CONTENTS (Continued)

	Page
5.5 Simulation Results.....	118
5.5.1 Simulation Results of Rectifier Side.....	118
5.5.2 Simulation Results of DC Bus.....	120
5.5.3 Simulation Results of Inverter Side.....	122
5.5.4 Simulation Results of MMC-based HVDC Systems.....	124
5.6 Harmonic Analysis.....	128
5.6.1 The Total Harmonic Distortion Requirements.....	128
5.6.2 Harmonic Analysis.....	129
5.7 Conclusions.....	130
VI DYNAMIC RESPONSE IMPROVEMENT OF VSC-HVDC CONTROLLER.....	
6.1 Introduction.....	142
6.2 Dynamic Response.....	142
6.2.1 Ziegler and Nichols Method.....	142
6.2.1.1 Proportional Controller.....	143
6.2.1.2 Integral Controller.....	144
6.2.2 Rule of Ziegler and Nichols.....	147
6.2.2.1 Closed-Loop Method.....	147
6.2.2.2 Open-Loop Method.....	149

TABLE OF CONTENTS (Continued)

	Page
6.2.3 Transient Performance and PI tuning of Inverter-side	150
6.3 Improved of Dynamic Response.....	150
6.4 Particle Swarm Optimization Method.....	154
6.5 The Simulation Systems and Simulation Results.....	157
6.6 Performance Analysis.....	161
6.7 Conclusions.....	164
VII CONCLUSIONS	166
7.1 Introduction.....	166
7.2 Conclusions.....	166
7.3 Future Research.....	168
REFERENCES	169
APPENDIX List of Publications.....	183
BIOGRAPHY.....	185

LIST OF TABLES

TABLES	Page
4.1 Switching angles versus to the modulation index of 27-level converter.....	97
4.2 Harmonic Requirements.....	98
5.1 Voltage distortion limits.....	128
5.3 The comparison of THD of multilevel converter.....	140
6.1 Closed-Loop Method.....	148
6.2 Open-Loop Method.....	150
6.3 PI parameters are searching by PSO.....	157
6.4 The overshoot performance of control systems are compared by PI tuning methods.....	161
6.5 The performance characteristic of MMC-based HVDC control system.....	163

LIST OF FIGURES

Figure		Page
1.1	Top ten countries had cumulative installed wind power generation by capacity in MW.....	5
1.2	Global cumulative installed wind capacity.....	6
1.3	Offshore wind energy potential is suitable for offshore wind farm.....	7
2.1	Schematic diagrams of HVDC transmission systems (a) LLC-HVDC and (b) VSC-HVDC.....	17
2.2	The mercury arc valve-based LLC-HVDC systems.....	18
2.3	The thyristor-based LCC-HVDC systems.....	19
2.4	The CCC-HVDC systems.....	19
2.5	The VSC-HVDC systems.....	19
2.6	The three-phase 12-pulse mercury arc valve-based LLC-HVDC systems.....	22
2.7	The three-phase 12-pulse thyristor-based LLC-HVDC systems.....	22
2.8	The DC voltage of 12-pulse converter.....	23
2.9	The AC currents of 12-pulse converter.....	23
2.10	Back to back LLC-HVDC Systems.....	26
2.11	Mono-polar LLC-HVDC systems.....	27
2.12	Bipolar LLC-HVDC systems.....	27

LIST OF FIGURES (Continued)

Figure	Page
2.13 Parallel connected multi-Terminal HVDC systems	27
2.14 Classical SPWM with triangular carriers	29
2.15 Carrier-shifted SPWM	30
2.16 Phase Disposition SPWM	30
3.1 General Configuration of DFIG	36
3.2 The Power Coefficient Curves with Different Pre-setting Pitch-angle	37
3.3 The Control Diagram of Blade Pitch-angle Controller	38
3.4 Driving train (a) The three-mass model and (b) The two-mass model	39
3.5 The Second-stage Current Controller for Rotor-side VSC	47
3.6 First-stage Power Controller for Rotor-side VSC	48
3.7 Diagram of grid-side converter	49
3.8 Second-stage Current Controller for Grid-side VSC	51
3.9 First-stage DC Voltage Controller for Grid-side VSC	52
3.10 Configuration of PMSG System	53
3.11 Second-stage Current Controller for Generator-side Converter	57
3.12 First-stage Controller for Generator-side Converter	58
3.13 First-stage VSC controller of WT-PMSG system	60
3.14 Layout of and Offshore Wind Farm Interconnected with External Power System	61
3.15 Network Reduction of One Chain in the Offshore Wind Farm	65

LIST OF FIGURES (Continued)

Figure		Page
3.16	The WT-DFIG Simulatin Diagram	72
3.17	The voltage characteristic on the Bus 575	73
3.18	The current characteristic on the Bus 575	73
3.19	The voltage characteristic on the Bus 25	74
3.20	The current characteristic on the Bus 25	74
3.21	The active power is generated by wind turbine	75
3.22	The reactive power is generated by wind turbine	75
3.23	The DC voltage characteristic	76
3.24	The turbine speed characteristic	76
3.25	The PMSG wind farm diagram	78
3.26	The voltage characteristic on bus 25 kV	78
3.27	The current characteristic on bus 25	79
3.28	The voltage characteristic on bus 575 V	79
3.29	The voltage characteristic on bus 575 V	79
3.30	The active power	80
3.31	The reactive power	80
3.32	The DC-bus voltage	80
3.33	The rotor speed	81
4.1	Single-phase MMC configuration	83
4.2	The Step-waveform	87
4.3	Switching angles versus modulation index of 7-level converter	91

LIST OF FIGURES (Continued)

Figure		Page
4.4	Cost function versus modulation index of 7-level converter.....	91
4.5	Cost function versus modulation index of 7-level converter.....	92
4.6	Harmonic amplitudes of 7-level converter ($M = 0.85$).....	93
4.7	Switching angles versus modulation index of 15-level converter.....	93
4.8	Line voltage total harmonic distortion versus modulation index of 15-level converter.....	94
4.9	The harmonic amplitudes of 15-level converter ($M = 0.85$).....	94
4.10	The switching angles versus modulation index of 27-level converter..	95
4.11	The line voltage THD versus modulation index of 27-level converter.....	95
4.12	The harmonic amplitude of fundamental harmonic of 27-level converter ($M=1.0$).....	96
5.1	The General Configuration of Point-to-point VSC-HVDC System.....	100
5.2	The Diagram of Rectifier-side Circuit.....	101
5.3	The Diagram of Inverter-side Circuit.....	104
5.4	The Diagram for Outer Power Control of Rectifier-side VSC Controller.....	109
5.5.	The Diagram of Inverter-side VSC Controller.....	111
5.6	The Diagram of Offshore Wind Farm.....	113
5.7	The Diagram of 3-level VSC-HVDC Offshore Wind Farm.....	113
5.8	The MMC based VSC diagram.....	115
5.9	Phase-lock-loop block diagram.....	115

LIST OF FIGURES (Continued)

Figure		Page
5.10	The measured points and control systems.....	116
5.11	MMC pulse controller.....	116
5.12	The Carrier-Shift SPWM.....	117
5.13	The measured active power and its referent on bus 1.....	119
5.14	The measured reactive power and its referent on bus 1.....	119
5.15	The measured voltage on bus 1.....	119
5.16	The measured current on bus 1.....	119
5.17	The measured d – axis control current and its referent on bus 1.....	120
5.18	The measured q – axis control current and its referent on bus 1.....	120
5.20	Simulation results; DC voltages.....	121
5.21	The measured DC voltages and its referent.....	121
5.22	The measured DC power.....	121
5.23	The measured d – axis control current and its referent on bus 2.....	114
5.24	The measured q – axis control voltage and its referent on converter bus 2	123
5.25	The active power on bus 2.....	123
5.26	The measure reactive power and its referent on bus 2.....	125
5.27	The voltage characteristic on bus 2.....	123
5.28	The current characteristic on bus 2.....	124
5.29	The AC voltage waveform for 73-level MMC.....	124

LIST OF FIGURES (Continued)

Figure		Page
5.30	The AC voltage waveform of MMC-based HVDC at the Bus 2.....	125
5.31	The AC voltage waveform of MMC-based on bus 2.....	125
5.32	The active power on bus 2.....	126
5.33	The measure reactive power and its referent on bus 2.....	126
5.34	The three phase voltage characteristic on the Bus 2.....	126
5.35	The three phase current characteristic on the Bus 2.....	127
5.36	The modulation technique of Carrier-shifted SPWM.....	127
5.37	The AC voltage waveform of OHSW method for 73-level MMC-based VSC-HVDC transmission system.....	128
5.38	The harmonic distortion of 3-level VSC is modulated PWM method, THD=73.2%.....	129
5.39	The phase to phase voltage harmonic is measured of 9-level MMC inverter is modulated by Carrier-shifted SPWM, the THD = 21.5%	130
5.40	The three phase line-to-neutral output voltage of 11-level MMC inverter is modulated by Carrier-shifted SPWM.....	130
5.41	The phase to phase output voltage of 11-level MMC inverter is modulated by Carrier-shifted SPWM.....	131
5.42	The phase to phase voltage harmonic is measured of 11-level MMC inverter is modulated by Carrier-shifted SPWM, the $THD_V = 7.3\%$	131

LIST OF FIGURES (Continued)

Figure	Page
5.43	The output voltage waveform of 15-level MMC inverter is modulated by Carrier-shifted SPWM, (a) the three-phase waveforms, (b) the line-to-line waveform 132
5.44	The output voltage waveform of 27-level MMC inverter is modulated by Carrier-shifted SPWM, (a) the three-phase waveforms, (b) the line-to-line waveform 133
5.45	The output voltage waveform of 73-level MMC inverter is modulated by Carrier-shifted SPWM, (a) the three-phase waveforms, (b) the line-to-line waveform 133
5.46	The output voltage waveform of 101-level MMC inverter is modulated by Carrier-shifted SPWM, (a) the three-phase waveforms, (b) the line-to-line waveform 134
5.47	The line-to-line voltage harmonic contents of 15-level MMC inverter 134
5.48	The line-to-line voltage harmonic contents of 27-level MMC inverter 135
5.49	The line-to-line voltage harmonic contents of 73-level MMC inverter 135
5.50	The line-to-line voltage harmonic contents of 101-level MMC inverter 135
5.51	The output voltage waveform of 11-level MMC inverter is modulated by OHSW method, (a) three-phase waveforms, (b) line-to-line voltage waveform 136

LIST OF FIGURES (Continued)

Figure		Page
5.52	The output voltage waveform of 15-level MMC inverter is modulated by OHSW method, (a) three-phase waveforms, (b) line-to-line voltage waveform	137
5.53	The output voltage waveform of 27-level MMC inverter is modulated by OHSW method, (a) three-phase waveforms, (b) line-to-line voltage waveform	138
5.54	The line-to-line voltage harmonic of 11-level converter (OHSW)	143
5.55	The line-to-line voltage harmonic of 15-level converter (OHSW)	144
5.56	The line-to-line voltage harmonic of 27-level converter (OHSW)	146
6.1	The Ziegler and Nichols Method (a) open-loop nonlinear system, and (b) Unity-feedback nonlinear system	143
6.2	The Ziegler and Nichols Method (a) Integral windup and (b) Anti-Integral windup	146
6.3	Closed-Loop Method of Ziegler and Nichols (a) Quarter-decay response (b) Ultimate gain and period	148
6.4	The unit-step response	149
6.5	The system performance (a) overshoot, (b) no over-shoot	151
6.6	The VSC controller system	152
6.7	The comparison of the performance response of the four criteria errors	153

LIST OF FIGURES (Continued)

Figure		Page
6.8	The simulation results of the output voltages when subjecting to input (a) the mean voltage in per unit on bus 2, (b) the three phase voltage on bus 2 and (c) the three phase voltages are generated by MMC.....	159
6.9	The output voltages when disturbance at $t = 0.5$ second and clearing at $t = 0.53$ second.....	160
6.10	Unit-Step response performance characteristics.....	163

CHAPTER I

INTRODUCTION

1.1 Background

The electrical energy demand is rapidly grow continuous. However, the increases in energy consumption have been met, to a large extent, by building new conventional power plants, particularly those that burn fossil fuels. This has resolved the pressing issue of electrical energy demand but has led to excessive and dangerous levels of carbon di oxide (CO_2) emissions into the atmosphere. Recent estimates of CO_2 emission of the electrical energy production industry at more than 40% of the total global (Rodriguez, M. F., 2012)

For this reason, a new generation of power plants has been introduced which produce electricity by using primary energy resources which are said to be renewable energy, such as wind, solar, geothermal and biomass. This had not the benefit of reducing CO_2 emissions into the atmosphere to a oppression only, but the new power plants to also stimulate a great deal of advance technological in both in research institutions and the manufacturing sector.

Today, the wind power is proven the most advanced from of renewable energy generation and economic advantages, in the United State of America, Investment Tax Credits (ITC) were introduced to promote the development of new technologies in the renewable energy sector and to bring down the competitive barrier with the conventional electricity power generation (Novogradac, M. J., 2010). In Europe, wind project have been supported from the profits side by feed-in premium and fee-in

tariffs (FIT) which are over electricity market prices (US-EU, 2011). The past decade, the wind farms have grown in size and the number of wind power installations has multiplied rapidly. The wind turbines are installed in Thailand bringing its up to 223 MW in total (Global Wind Energy Council, 2015).

1.2 Motivation

1.2.1 Wind Farm Applications

Recently, the wind farms have been grown rapidly. Therefore, the unit size up to about 1MW, most of the windmills is fixed speed asynchronous generators that are directly couple to the power grid and have stall control of the blades. This option has some disadvantages because generators operating at fixed speed, driven at the fixed grid frequency, cause variations of the output power according to the wind speed. Consequently, the grid voltage is very unstable especially with weak AC systems. This, and overload protection, were the main motive to change the windmill technology from fixed speed to variable speed generators when the unit size was increased to the MW level (Rodriguez, M.F., 2012).

The design of a variable speed windmill needs a converter is connected between the generator and the grid. This converter is designed, in most cases, as an IGBT-Base VSC. There are several different solutions available for the generator:

1. Fully-fed synchronous generator, optionally with permanent magnet excitation
2. Fixed speed, active stall, regulated wind turbines driving asynchronous generators.

3. Variable speed pitch regulated wind turbines driving double fed asynchronous generators.

The converter required for each solution is different: Fully-Fed means that the converter rating is equal to the generator size is connected at the stator windings. Double-Fed means that the converter is rating is about 25% of the generator size is connected at the rotor winding via slip rings. But, with respect to the line-side behavior, there is no different when we see the generator-converter system as one unit.

The main characteristics of windmills, operating with variable speed generators interfaced by busing converters, and pitch control are as follows:

1. According to specification, the windmill unit is designed for a power factor between 0.9 capacitive and 0.9 inductive and this can be controlled in a dynamic way. Reference values have to be supplied by the energy management computer. This design of the generator-converter system achieve a reactive power control in range of $\pm 50\%$ of the full load, active power available which can be used for cabling optimization and grid voltage control/stabilization.
2. The waveform of voltage and current are nearly sinusoidal, and no extra filters outside the converter are needed.
3. The converter limits the output power to the rated power.
4. Each windmill is connected to the local grid through the line transformer and so an existing grid voltage level can be adopted.
5. The active power of the windmill is controlled by pitch controller by varying the angle of the blades.

For the offshore wind farm, owing to the high cost of the foundation and other offshore facilities, wind farm developers will usually install the largest wind mills possible. However, due to the present day blade material technology, the maximum limit to the power output is about 5MW.

To reduce in impact from windmill to windmill due to wind turbulence, the distance between two windmills should be about 700 m as far as possible. That means a 500 MW wind farm, with 100 windmills as 5 MW each, need an area of $7 \times 7 \text{ km}^2$. All windmills are connected to a local 30 kVAC grid in star configuration or a combination of them. A substation with HV switchgears and power transformer will be the local point of common coupling (PCC) for the power transmission line to onshore power systems. AC/DC systems can both do this. However, at first side, the simplest one appears to be AC transmission because the offshore wind farm needs auxiliary energy when the wind is not blowing, and all the essential equipment is already well known and existing. Respecting, existing cable technology, the capacity of a 3-core AC submarine cable is presently about 200 MW at 145 kV.

Because the number of cables has to be reduce. HVDC technology should be decided. That implies using the well-known conventional HVDC technology. (Kim C. K., et al, 2009).

US Department of Energy had reported that the global wind additions yet again reached a new high in 2015, with roughly 63,000 MW of new capacity, 23% above the previous record of 51,000 MW added in 2014. Cumulative global capacity stood at approximately 434,000 MW at the end of 2015. The top ten countries had cumulative installed wind power generation is shown in Figure 1.1 and the global cumulative installed is shown in Figure 1.2 (Wiser, R. and Bolinger, M., 2016)

The United State leading the world ranging in annual wind power capacity additions from 2005 through 2008, and then losing to China from 2009 through 2011, and the narrowly regained the global ranging in 2012. In 2013, the annual addition of United States is dropped to 6th place in ranging, but then regained ground, rising to 3rd in 2014 and 2nd place ranging in 2015. The U.S. wind power market represented 14% of global installed capacity in 2015.

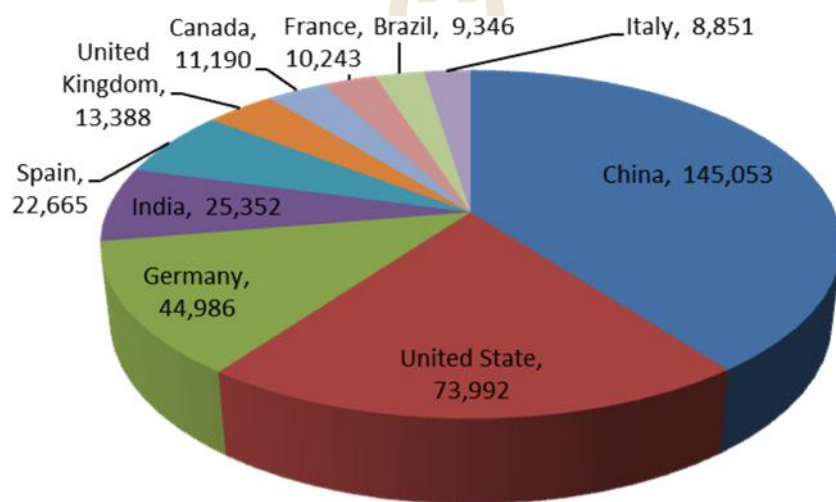


Figure 1.1 Top ten countries had cumulative installed wind power generation by capacity in MW

A number of countries have achieved relatively high levels of wind energy penetration in their electricity grids. Figure 1.2 presents data on end-of-2015 installed wind power capacity, translated into projected annual electricity supply based on assumed country-specific capacity factors and then divided by projected 2016, electricity consumption. Using this approximation for the contribution of wind power to electricity consumption, and focusing only on those countries with the greatest

cumulative installed wind power capacity, end-of-2015 installed wind power is estimated to supply the equivalent of roughly 40% of Denmark's electricity demand, and Portugal, Ireland, and Spain's demand are between 20% to 30%. In the United States, the wind power installed at the end of 2015 is estimated equate to 5.6% of the nation's electricity demand. On a global basis, wind energy's contribution is estimated to be approximately 4.3%.

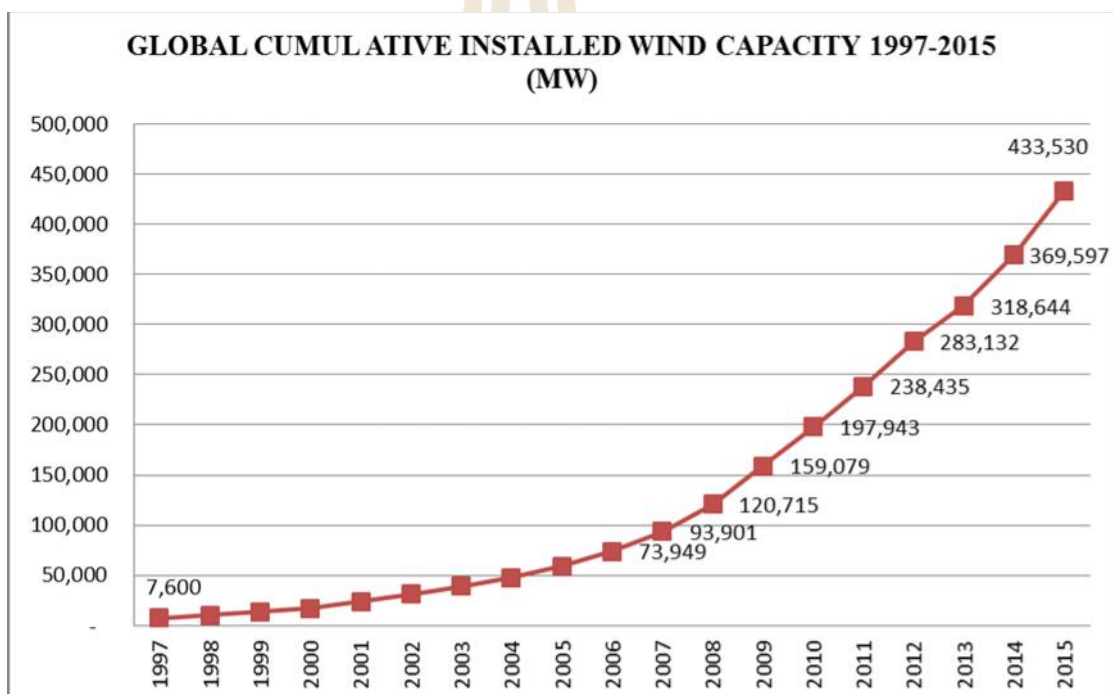
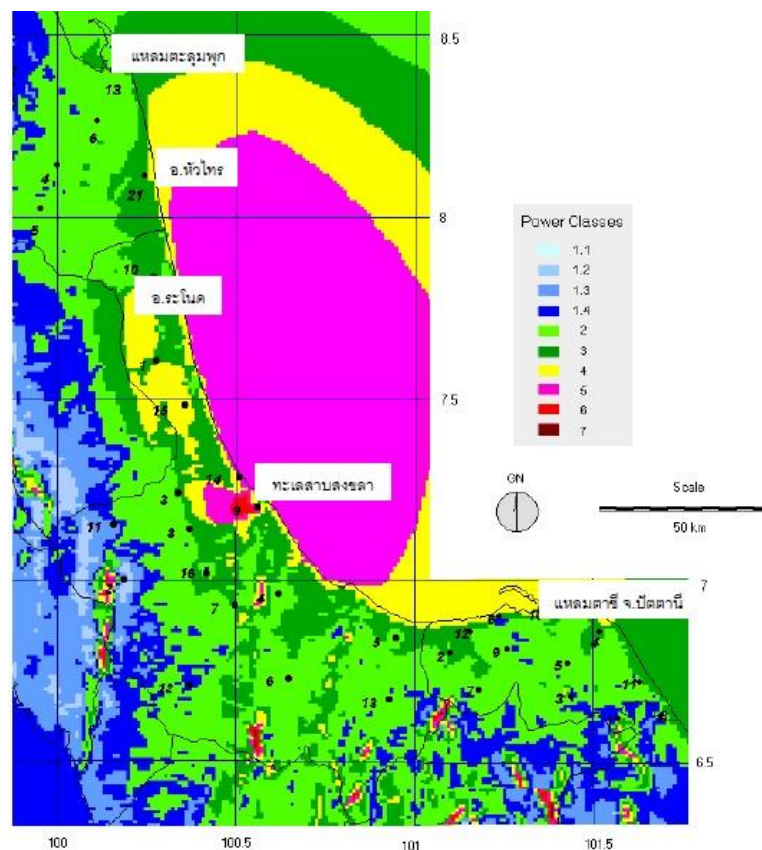


Figure 1.2 Global cumulative installed wind capacity

1.2.2 Wind Turbine Applications in Thailand

The first study of wind energy potential in Thailand was conducted in 1975 by the Department of Alternative Energy Development and Efficiency. In 2011,

Silpakorn University researcher to improve the wind map. The research produced the wind maps with resolution of $3 \times 3 \text{ km}^2$ cells using atmospheric model and computer simulation software and also experimented with the making of micro-scale wind maps. For offshore wind potential in Thailand, there are some areas with high wind speeds for example Bandon Bay in Surat Thani Province, Songkhla Gulf and Songkhla Lake in Songkhla Province, the potential of offshore wind is shown in Figure 1.3. Thailand had its first pilot project by EGAT at Laem Phromthep in Phuket Province, consisting of six turbines. As of the end of 2014, Thailand's wind power is installed at 224.5 MW and it is generated the 305 GWh energy per a year, the wind power capacity is 46th in the world ranging.



		THAILAND WIND POWER CLASSES										
Elevation		1.1	1.2	1.3	1.4	2	3	4	5	6	7	
10 m	m/s	0	2.8	3.6	4.0	4.4	5.1	5.6	6.0	6.4	7.0	9.4
	W/m ²	0	25	50	75	100	150	200	250	300	400	1,000
30 m	m/s	0	3.3	4.1	4.7	5.2	5.9	6.5	7.0	7.4	8.2	11.0
	W/m ²	0	40	80	120	160	240	320	400	480	640	1,600
50 m	m/s	0	3.6	4.4	5.1	5.6	6.4	7.0	7.5	8.0	8.8	11.9
	W/m ²	0	50	100	150	200	300	400	500	600	800	2,000

Figure 1.3 Offshore wind energy potential is suitable for offshore wind farm

1.2.3 HVDC Transmission Systems

For traditional AC power system, effective utilization of power from renewable sources is hindered by factors such as its intermittency nature, distance from the renewable source to the load center, distance between two or more power systems, frequencies difference between the two power systems and the complexity of the power system network. The high voltage direct current (HVDC) technology is one of the effective techniques that had been widely used to solve these problems (Brenna, M., Foadelli, F., Longo, M., and Zaninelli, D., 2017). The beginning development of HVDC transmission systems dates back when Peter Cooper Hewitt invented the mercury-arc valve or mercury-arc rectifiers in 1902. This technology is developed by both North American and European researchers in the duration times between the 1920s and 1930s. For this reason, the mercury-arc stations were used for the DC power systems in USA urban of Thomas Edison. However, the mercury arc valves were replaced by semiconductor devices for used in the rectifier technology in 1970s (Tiku, D., 2014). The line-commutated converters which are the basic converters were used at the sending and receiving end stations are called LCC- HVDC transmission

systems. (Radzuan, R., Raop, M. A. A., Salleh, M. K. M., Hamzah, M. K. and Zawawi, R. A., 2012).

According to the development of power electronic devices and advantages of HVDC transmission systems, the applications of HVDC are more important in high voltage transmission systems. The previously applications of HVDC are used transmitting the electrical energy from long distance of two location areas, interconnect renewable resources located far away from consumption centers, the two systems are different frequencies and to integrate electricity markets over large geographic areas, the system configurations and technologies are according the either objective in any project. The both thyristor-based LCC-HVDC and IGBT-based VSC-HVDC are parallel used. The decisions are according the objectives, locations and prices.

The newest technology for HVDC that is VSC-HVDC systems is addressed. The thyristor-based LCC-HVDC systems and VSC-HVDC systems are suitable for applications depending on different purposed characteristic, power capacity and distance between the two systems. It has shown that HVDC configurations depend on the function and location of converter stations. The back-to-back HVDC system is part of this work. It is also expressed that in the Point-to-point HVDC systems can either be monopolar or bipolar HVDC systems and for the multi-terminal HVDC systems there are more than two power converter stations connected. Several methods for controlling the firing angle of the thyristor for LCC-HVDC converter are explained. There are two methods that have been widely used, IPC and EPC. For VSC-HVDC converters, a very popular high switching frequency SPWM that has been widely used.

1.2.4 Harmonics and Control Systems Performances.

Harmonics are sinusoidal voltage or current having frequencies that are integer multiples of fundamental frequency. The total harmonic distortion (THD) is a growing concern for power system utilities because of increasing of power electronic equipment. To handle this concern, IEEE 519-2014, it provides guideline for harmonics voltage and current distortion level on transmission and distribution circuits. Therefore, recent research and applications in power electronic application for power systems is considered. This research is focused on the improvement the harmonics performance that generated by power electronic devices of HVDC transmission systems.

The performance of the control system is usually evaluated base on its transient response behavior. This response is the reaction when subjecting a control system to input or disturbance. The characteristics of the desired performance are usually specified in terms of the time domain quantities. Commonly, unit responses are used in the evaluation of the control system performance due to their ease of generation in practical control systems. The transient response often exhibits damped oscillations before reaching steady state. There are many time domain parameters which are used to evaluate the unit step response. This research is proposed dynamic response improvement of the VSC-HVDC controller by the adjustment the control systems of the PI controller, are proposed the conventional PI tuning and compared to the PI tuning by particles swarm optimization

1.3 Research Objectives and Methodologies

The main objective of this thesis is to improve the voltage total harmonic distortion of HVDC converters and to improve the dynamic response of VSC-HVDC control system. This thesis contributes the modular multilevel converter application for VSC-HVDC system and to compare the total harmonic distortion of SPWM and PSO optimized harmonic modulation methods. For the improvement the control system performance, this thesis is proposed the PSO optimization for searching the PI parameters and compared with conventional PI tuning. The main objectives of this thesis include:

1. To improve the modulation control of modular multilevel converter to achieve the good harmonic performance of VSC-HVDC for power system integrated with an offshore wind farm.
2. To improve of control system of MMC-based HVDC for power system integrated with an offshore wind farm to achieve the good dynamic response performance
3. To improve the modular multilevel converter model and control for HVDC applications for power system integrated with an offshore wind farm.
4. To verify and comparison the harmonic performance of the particle swarm optimization OHSW method and the SPWM modulation method for modulate of modular multilevel converter.
5. To verify and comparison the dynamic response performance of MMC-based HVDC transmission systems for power system integrated with an

offshore wind farm by using the particle swarm optimization and conventional PI tuning methods.

1.4 Scope and Limitation of the Thesis

The scope of this thesis is proposed the control systems for offshore wind farm is connected to the power system through VSC-HVDC transmission systems to improve the voltage total harmonic distortion and dynamic performance of VSC-HVDC control systems. The scope and limitation of this thesis include:

1.4.1 Scope of the Thesis

1. Improve the modulation technique and control of modular multilevel converter to achieve the good harmonic performance by using particle swarm optimization for power system integrated with an offshore wind farm through VSC-HVDC transmission system.
2. Verify and comparison the harmonic performance of the particle swarm optimization OHSW method and the conventional SPWM modulation method for modulate of modular multilevel converter applications for power system integrated with an offshore wind farm through VSC-HVDC transmission system
3. Improve of control system of MMC-based HVDC for power system integrated with an offshore wind farm to achieve the good dynamic response performance
4. Verify and comparison the dynamic response performance of MMC-based HVDC transmission systems for power system integrated with an

offshore wind farm by using the particle swarm optimization and conventional PI tuning methods

1.4.2 Limitation of the Thesis

1. Improve the modulation technique and control of achieve the good harmonic performance of modular multilevel converter by using particle swarm optimization and simulation by using MATLAB Program.
2. Verify by comparison the harmonic performance of particle swarm optimization method and the conventional SPWM modulation method and IEEE standard requirements by using MATLAB Program.
3. Comparison the harmonic performance of different level output voltage waveform of modular multilevel converter and IEEE standard requirements by using MATLAB and Simulink Program.
4. Apply and improve the control systems for simulation of the modular multilevel converter for power system integrated with an offshore wind farm through HVDC systems by using MATLAB and Simulink Program.
5. Verify and comparison the harmonic performance of MMC-based HVDC systems and IEEE standard requirements by using MATLAB and Simulink Program.
6. Improve of control system of MMC-based HVDC for power system integrated with an offshore wind farm to achieve the

good dynamic response performance by using MATLAB and Simulink Program.

7. Verify and comparison the dynamic response performance of MMC-based HVDC transmission systems for power system integrated with an offshore wind farm by using the particle swarm optimization and conventional PI tuning methods by using MATLAB and Simulink Program

1.5 Thesis Outline

The work present in this thesis is divided into the following chapters.

Chapter 1: Introduction. This chapter is presented the background and the motivation of research, the objectives and methodology of research, Scope and limitation of thesis and Thesis outline.

Chapter 2: Literature review. This chapter is present the state of arts of the thesis

Chapter 3: Modeling and control of wind turbines. This chapter is presented the modeling and control of both DFIG and PMSG variable speed wind turbines, and then the aggregated modeling method for large-scale offshore wind farms consisting of DFIGs and PMSGs.

Chapter 4: Particle Swarm Optimized Harmonic for Modular Multilevel Converter. This chapter is presented about the optimized harmonic stepped waveform for modular multilevel converter by using particle swarm optimization.

Chapter 5: Modeling and Control of MMC-Based HVDC Transmission Systems. This chapter present about the modeling and control of modular multilevel

converter for power system integrated with an offshore wind farm through HVDC systems. Otherwise, apply and improve the control systems for simulation of the modular multilevel converter for power system integrated with an offshore wind farm through HVDC systems. To verify the harmonic performance of MMC-based HVDC systems by compared with IEEE standard requirements and conventional methods.

Chapter 6: Dynamic Response Improvement of VSC-HVDC controller. This chapter to improve the dynamic response of VSC-HVDC controller by PI parameters tuning using particle swarm optimization and compare with the conventional ITAE, ISE, ITSE and Ziegler & Nichols method

Chapter 7: Conclusions, this chapter is present the thesis conclusions and future work.

CHAPTER II

LITERATURE REVIEW

2.1 Introduction

This chapter discusses the state of art on several topics relevant to this thesis. First of all, overview of multilevel converter topologies and controls and then, review of wind power generation technologies and HVDC transmission systems, and finally review the state of arts of power system control for stability enhancement.

2.2 Review of HVDC Transmission Systems

For traditional AC power system, effective utilization of power from renewable sources is hindered by factors such as its intermittency nature, distance from the renewable source to the load center, distance between two or more power system, frequencies difference between the two power systems and the complexity of the power system network. The high voltage direct current (HVDC) technology is one of the effective techniques that had been widely used to solve these problems (Xie, H., Bie, Z., Lin, Y., and Zheng, C., 2017). The beginning development of HVDC transmission systems dates back when Peter Cooper Hewitt invented the mercury-arc valve or mercury-arc rectifiers in 1902. This technology is developed by both North American and European researchers in the duration times between the 1920s and 1930s. For this reason, the mercury-arc stations were used for the DC power systems in USA urban of Thomas Edison. However, the mercury arc valves were replaced by

semiconductor devices for used in the rectifier technology in 1970s (Tiku, D., 2014). The line-commutated converters which are the basic converters were used at the sending and receiving end stations are called LCC- HVDC transmission systems. (Radzuan, R., et al, 2012)

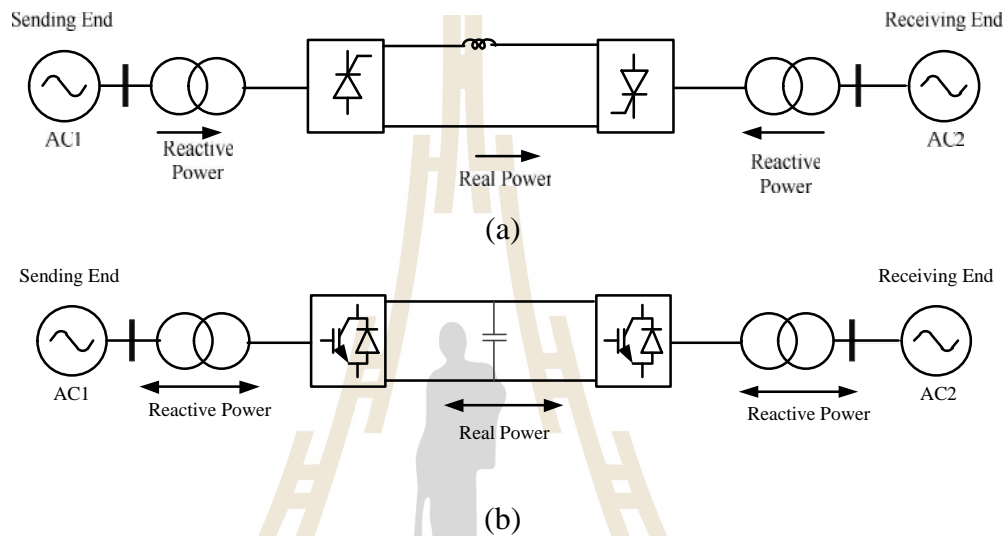


Figure 2.1 Schematic diagrams of HVDC transmission systems (a) LCC-HVDC and (b) VSC-HVDC

However, the control process of thyristor can only turn-on, and rely turn-off by the external AC system, the control system only has one degree of freedom when turning-on the thyristor. Because of these limitations of thyristor it means that the AC system to which the LCC-based HVDC is connected with must always contain synchronous machines for provide the commutating voltage. Moreover, it cannot control the power for the all P-Q operation plan. This disadvantage was solved by the development of the insulated-gated bipolar transistor (IGBT) enabling both turn-on and turn-off process. As a result, IGBT can be used to make self-commutated converters for HVDC applications called voltage source converters based HVDC or VSC-HVDC systems (Janjamraj, N., Oonsivilai, A., 2013). The schematic of two

types of HVDC systems with different power electronic technologies are shown in Figure 2.1.

2.3 HVDC Classifications

After the initial mercury arc based HVDC is terminated, the modern HVDC is based on power electronic devices. The first thyristor based HVDC installation is Eel River project in Canada and it went into services in 1972. After that, the HVDC application in AC transmission system has established itself as an important part of power system planning. Recently, due to important developments in power electronic devices, there is much ongoing researches related to Flexible AC Transmission Systems (FACTS), which provide system stability by controlling the active and reactive power (Xue, Y., and Zhang, X. P., 2017). It can be classified according to either power electronic technologies are the shown in Figure 2.2.

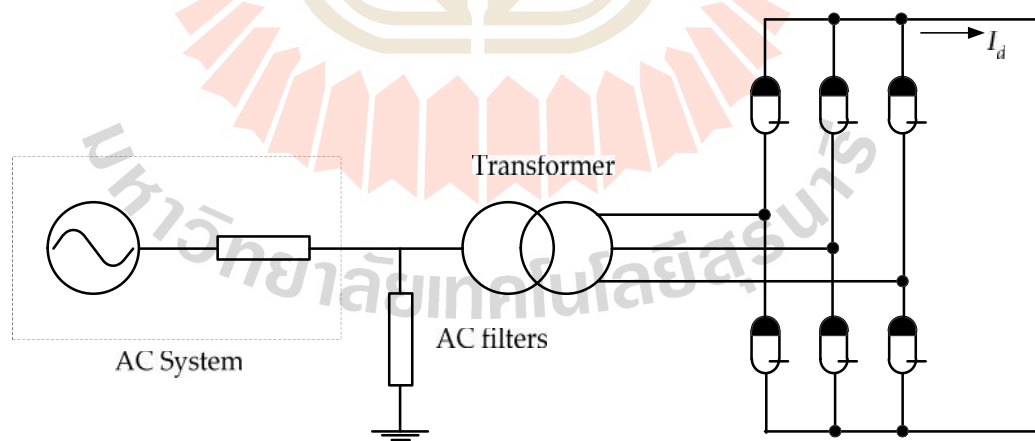


Figure 2.2 The mercury arc valve-based LLC-HVDC systems

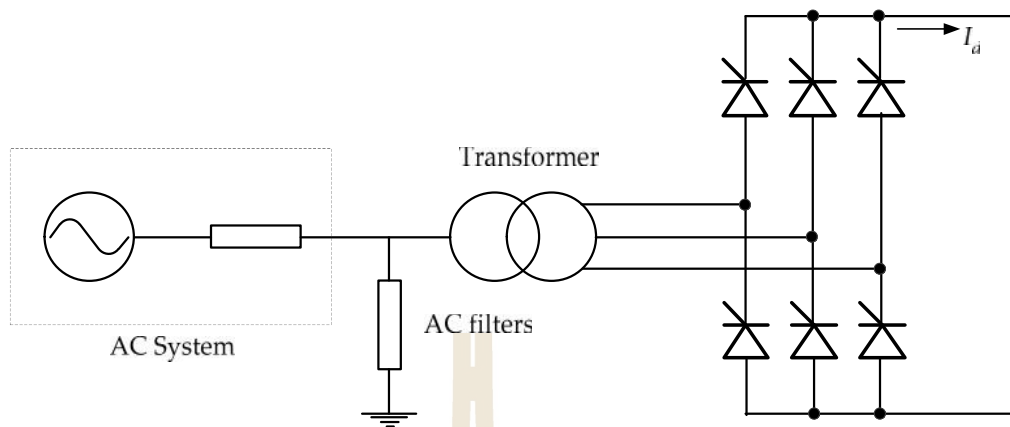


Figure 2.3 The thyristor-based LCC-HVDC systems

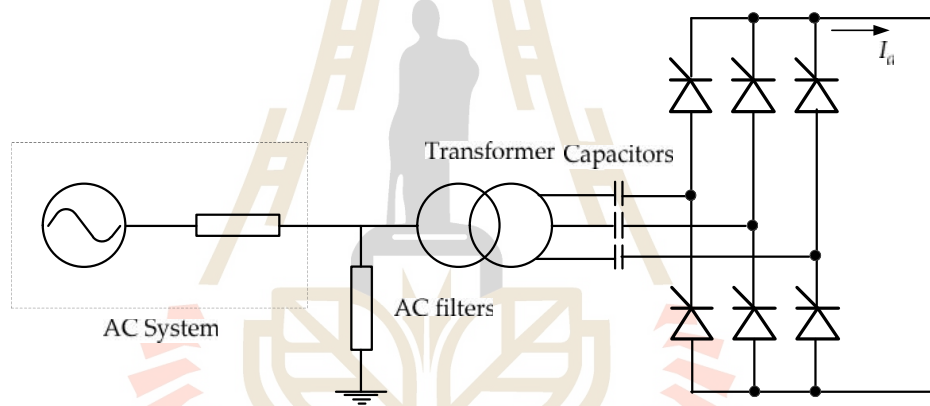


Figure 2.4 The CCC-HVDC systems

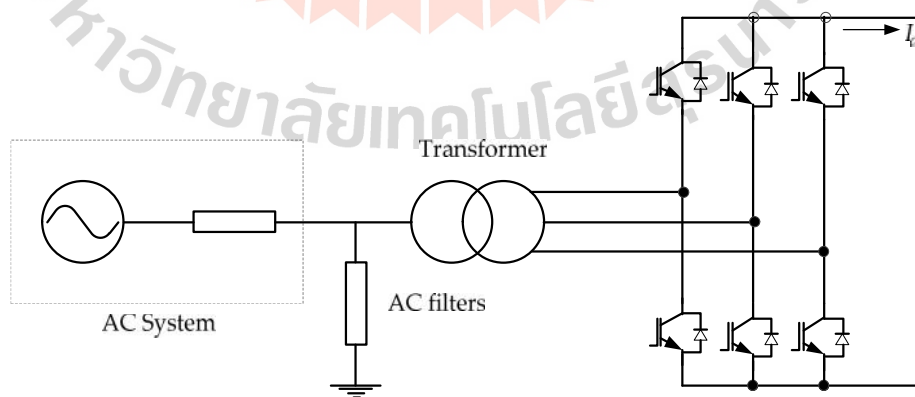


Figure 2.5 The VSC-HVDC systems

2.3.1 Mercury Arc Rectifier Based LCC-HVDC Systems

The first generation of HVDC transmission systems dates back to 1882 when Jemin and Meneuvier had recognized the behavior of unidirectional current flow in a mercury arc with atmospheric pressure (Dijkhuizen, F., 2012) and Peter Cooper Hewitt invented the mercury-arc rectifiers or mercury arc valves in 1902 for used to convert AC to DC. The structures of mercury arc valves are consist of tree or more electrodes are assembly in the glass tube. The operation principle of mercury arc valve is that, when vaporize the mercury in the tube heat up by the given current, the full power level could travel through the other side. The behaviors on the AC waveform is that, the current can through only first positive half cycle and prevent through back the negative half cycle, this effectively acting similar to a diode. The advantage of mercury arc valve is used for HVDC applications are used for rectified the power waveforms from AC systems to DC systems and it was robust and could handle high voltage (Prince, D. C., 1926). The basic configuration of mercury arc rectifier based LCC-HVDC application was 6-pulse bridge or Graetz-bridge converters and for smoother DC waveform and reduced the harmonic contents, the 12-pulse mercury arc converter was recommended. The configuration of 12-pulse mercury arc converter is shown in Figure 2.6.

2.3.2 Thyristor Based LCC-HVDC Systems

The major development of the LCC-HVDC transmission systems occurred when the solid-state devices were invented in 1960s. The thyristor valves, like mercury arc valves require connection to an external AC circuit to turn them on and off. The HVDC using thyristor valves is known as line-commutated converter or called thyristor based LCC-HVDC. The configuration of 12-pulse bridges converters

are shown in Figure 2.7.

Since its first application of LCC-HVDC in 60 years ago, the conventional LCC-HVDC technology has applied an important for long distance power transmission systems around the world. However, some well-known limitations associated with it still exist today which to a certain extent limit further applications of the technology. The LCC-HVDC systems are robustness but it had the limitations of in reactive power control at both sides of the HVDC system. The requirement of reactive power originates from the thyristors firing after commutation voltage becomes positive, which delay the current waveforms. For this has attracted the attention of many researchers to solve the problem and limitations of LCC-HVDC systems and LCC-HVDC applications.

The operation principles and its voltage and current of the 12-pulse LCC-HVDC converter are shown in Figure 2.7. The 12-pulse connection consists of two 6-pulse group, one group having Y-Y connected converter transformer, and the other group having a Y- Δ connected converter transformer. A series connection of the two 6-pulse groups constitutes a 12-pulse connection. The DC 6-pulse and 12-pulse converters are shown in Figure 2.8 and the current flow in the AC side winding of the converter transformers are shown in Figure 2.9.

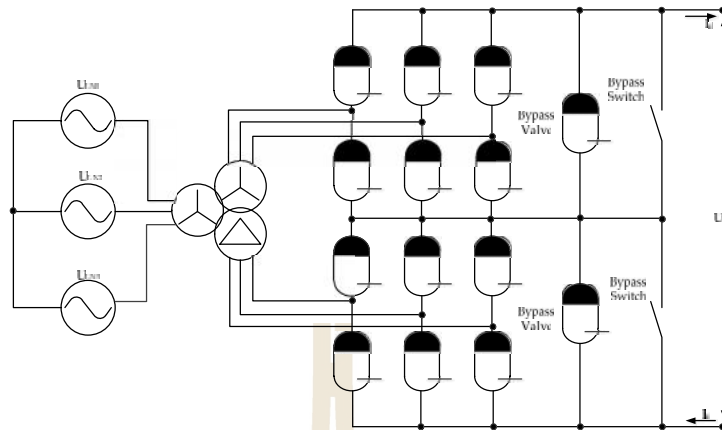


Figure 2.6 The three-phase 12-pulse mercury arc valve- based LLC-HVDC systems

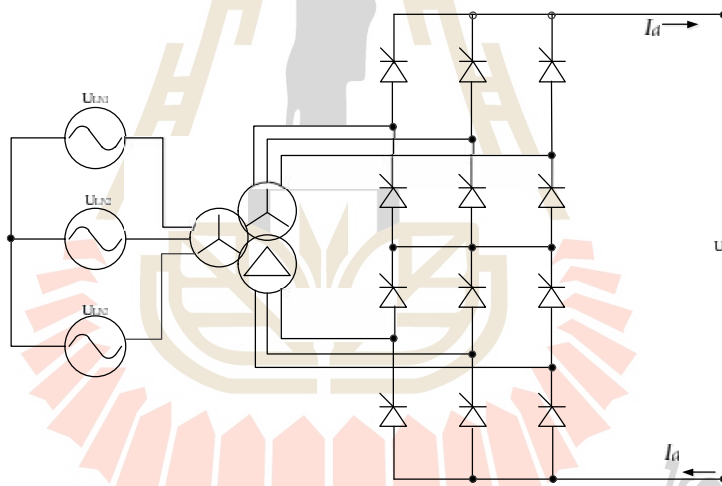


Figure 2.7 The three-phase 12-pulse thyristor- based LLC-HVDC systems

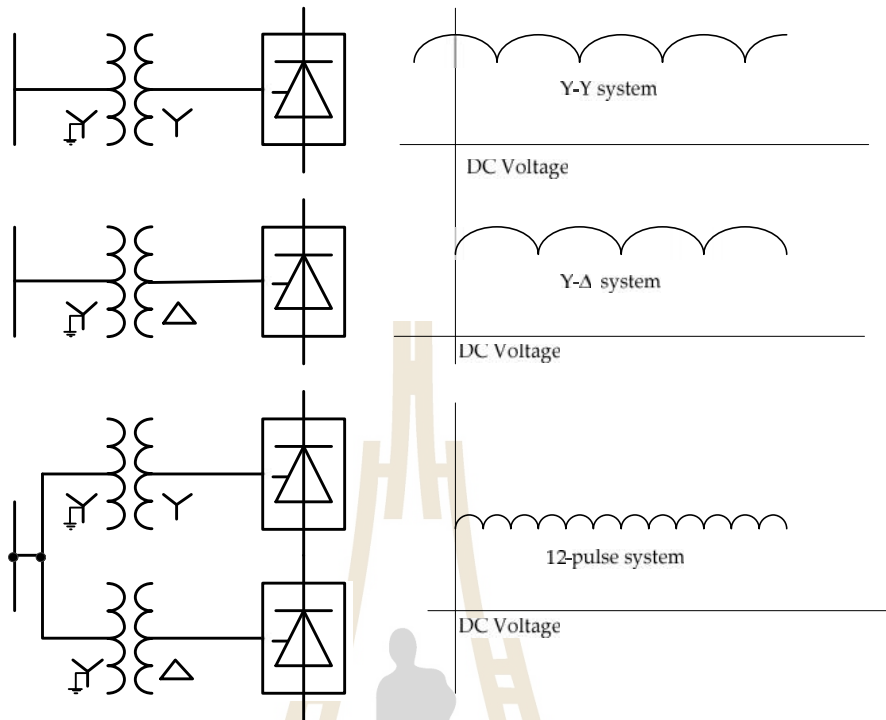
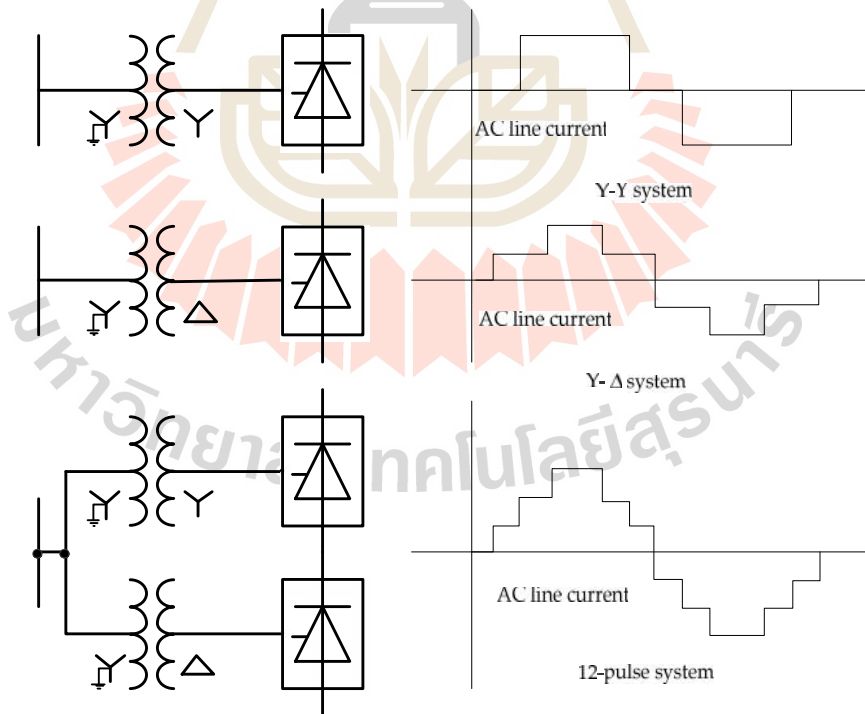


Figure 2.8 The DC voltage of 12-pulse converter



(b)

Figure 2.9 The AC currents of 12-pulse converter

2.3.3 CCC-HVDC Systems

For some limitations of the thyristor-based line commutate converter in their use for HVDC systems. This is resulted from requiring the AC circuit to turn-off the thyristor current and the need for a short period of reserve voltage to affect the turn-off time. An attempt to address these limitations is the application of Capacitor-Commutated Converter (CCC). The CCC-HVDC topology includes capacitors in series with the valve side transformer winding to offset the commutating inductance of the converter and help to reduce fault currents. However, the CCC-HVDC is not widespread because the disadvantages of LCC can be solved by the voltage source converter (Gao, T., and Ma, X., 2012)

2.3.4 VSC-HVDC Transmission Systems

The voltage source converters are widely used in motor drives since 1980s, this converter topology as the results of the development of semiconductor switching devices such insulated-gate bipolar transistor (IGBT). The first IGBT is proposed and practice in 1980s (Baliga, B.J., et al, 1982). The advantages of VSC that can be solved the disadvantage of LCC, it can be used to make self-commutated, available to control both turn-on and turn-off in many times per cycle in order to improve the harmonic performance.

The HVDC converter using IGBTs is usually referred to as a voltage source converter, that system is called VSC-HVDC system, it can feed active and reactive power to an AC network something which is impossible with LCC-HVDC and can be controlled the active and reactive power for all P-Q operation plan . The additional, VSC stations are also considered more compact than the LCC stations, therefore, suitable for location where space is at a premium, for example on offshore

platforms. It is widely used in motor drives since 1980s and started to be started commercially in HVDC application in 1997. The ABB is called this concept is HVDC Light while the similar concept by Siemen is called HVDC Plus. These converters has roughly paralleled with that for thyristor valve converters in the 1970s.

2.4 Review of HVDC Configurations

Because of, the applications of HVDC transmission systems are difference sites, locations, and purposed such as difference frequencies of two areas, long distance of two areas and transfer the electrical energy from offshore wind farms. Therefore, the HVDC configurations are depending upon the location, function and operating purposed of HVDC systems. Therefore, the HVDC systems are various classifications can be identified as below.

2.4.1 Back-to-back HVDC Systems

The main purposed of the Back-to-Back HVDC is used for two AC systems of similar or different frequencies can be connected. The configuration of back-to-back HVDC systems are included the two converter stations are located at the same site. There is no power transmission for a DC link over a long distance. The configuration of with 12-pulse converters back-to-back LCC-HVDC system is shown in Figure 2.10.

2.4.2 Point-to-point HVDC Systems

The general purposed of point-to-point HVDC systems are similar the back-to-back systems, but the both converter stations are not in same site areas. The overhead lines or submarine cables are used in this type of transmission system to connect the both converter stations. These systems can be either monopolar or bipolar.

The monopolar HVDC system had the two converters which are separated by a single pole line and a positive or a negative is used. Many of the cable transmissions with submarine connection and the ground for returning current are used. The block diagram of the 12-pulse monopolar LCC-HVDC system is shown in Figure 2.11.

For bipolar HVDC Systems, depicted in Figure 2.12, it is the most common LCC-HVDC system configurations where overhead lines are used to transmit power. A bipolar system comprises of two mono-polar ones. The advantage of this system is that one pole can continue to transmit power while the other is out of service. That means each system can operate on its own as an independent system with the earth return. Since one is positive and the other is negative, in case that both poles have equal currents, the ground current is theoretically zero. The block diagram of the 12-pulse bi-polar LCC-HVDC system is shown in Figure 2.12.

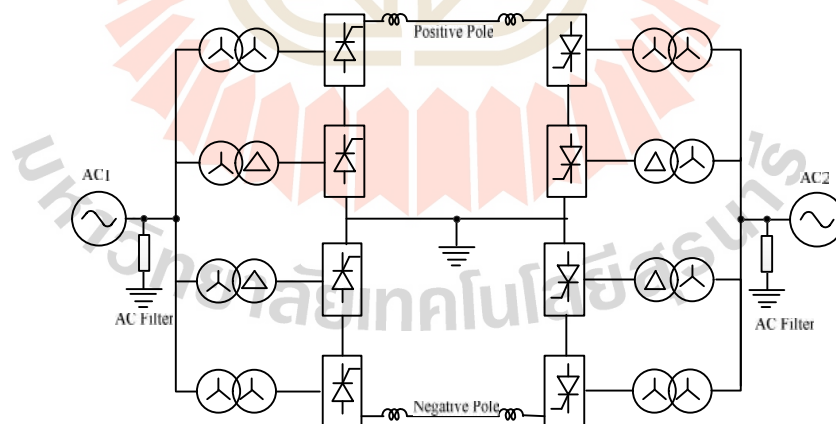


Figure 2.10 Back to back LLC-HVDC Systems.

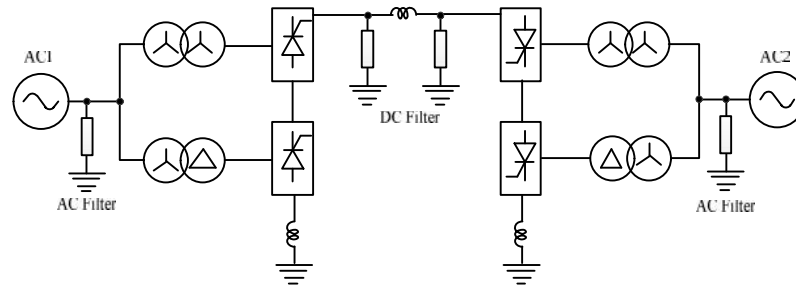


Figure 2.11 Mono-polar LLC-HVDC systems

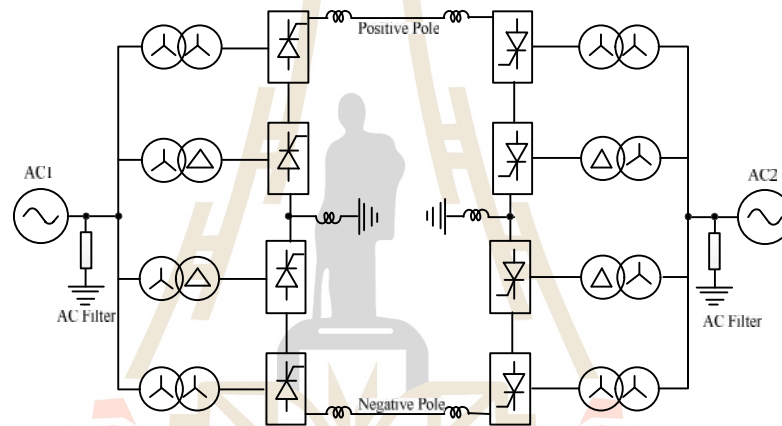


Figure 2.12 Bipolar LLC-HVDC systems

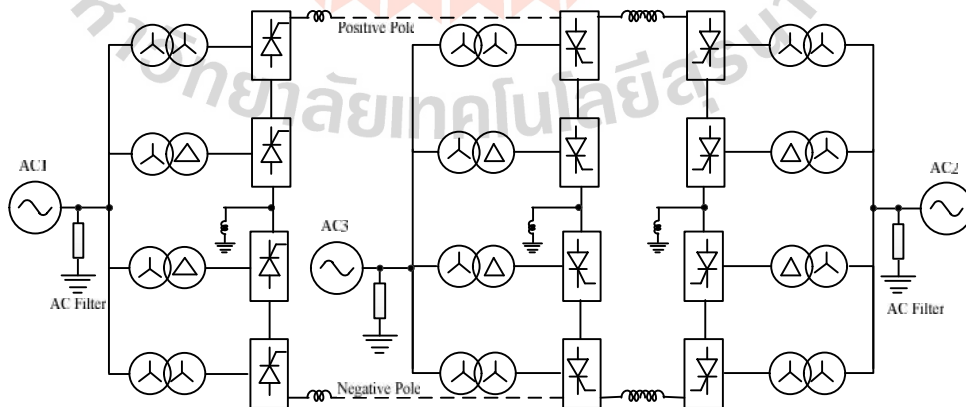


Figure 2.13 Parallel connected multi-Terminal HVDC systems

2.4.3 Multi-terminal HVDC systems

The multi-terminal HVDC system is called MTDC is an HVDC which more than two HVDC stations are interconnected with transmission lines. They are two kinds of MTDC systems are based on the difference of converter technologies, which voltage source converter is called VSC-MTDC and which line-commutated converter is called LCC-MTDC or thyristor-based MTDC. In the general, the MTDC can be arranged with different stations in series or in parallel, the configuration of 12-pulse converters per pole LLC-MTDC is interconnected in parallel is shown in Figure 2.13. In Recent, the VSC- MTDC is considered that suitable for HVDC due to easy and flexible for control of passive and active powers (Yuan, X. et al, 2015).

2.5 Review of Control of HVDC Transmission Systems

2.5.1 Converter Control for HVDC Systems

For the LCC-HVDC converters, there are many methods for controlling the firing angle of the thyristors. There are two methods that have been widely used. The first is based on the individual phase control (IPC) method and the other is based on the equidistant pulse control (EPC) method. These are the most commonly used (Siddiqui, M., and Bhatt, C., 2013). The IPC method was used in the early days of the HVDC transmission. It generates a control signal for each of the three phases independently. There are two types of the IPC, the linear turn-on method and \cos^{-1} method. The EPC turn-on method uses a phase locked oscillator to generate pulse with a constant time interval between each other. There are three types of such methods are Pulse Period Control, Pulse Frequency Control (PFC) and Pulse Phase Control (PPC).

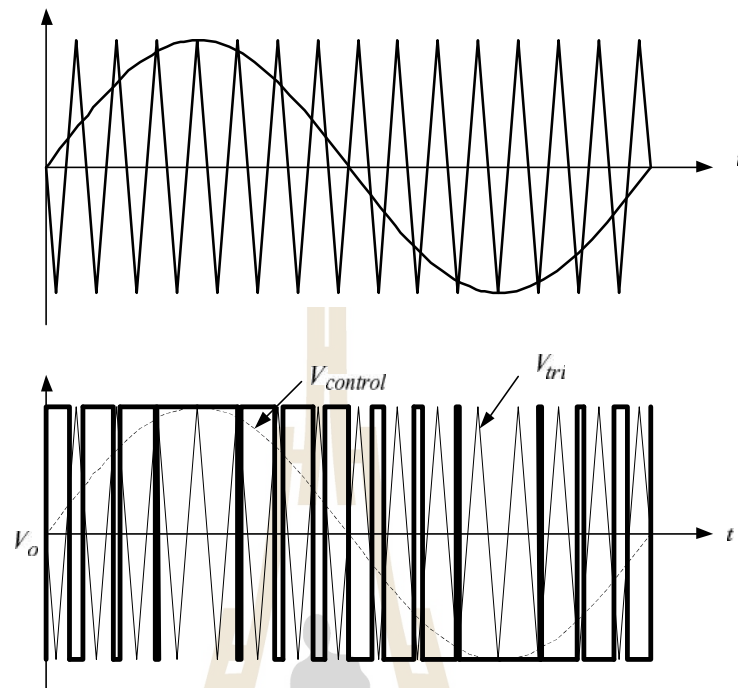


Figure 2.14 Classical SPWM with triangular carriers

For the control of VSC converters the two modulation methods can be classified according to switching frequency. The high switching frequency is very popular method in industrial applications (Tolbert, L., and Habetler, T.G., 1999), The first generation of high frequencies modulation techniques as shown in Figure 2.14, and several multicarrier techniques have been developed to reduce the distortion in multilevel inverters, Some methods use carrier disposition and others use phase shifting of multiple carrier signals as shown in Figure 2.15, and Phase disposition SPWM is shown in Figure 2.16.

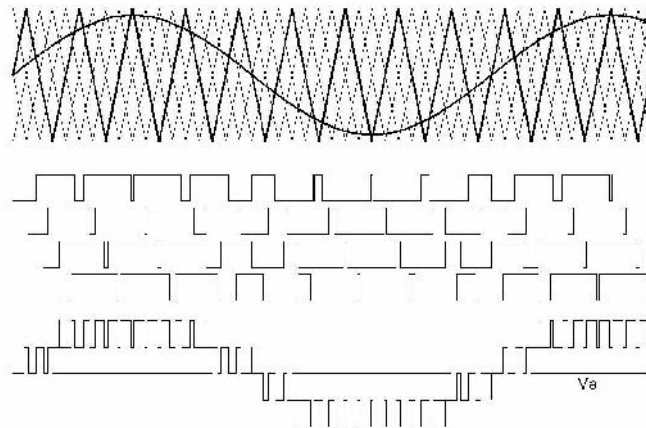


Figure 2.15 Carrier-shifted SPWM

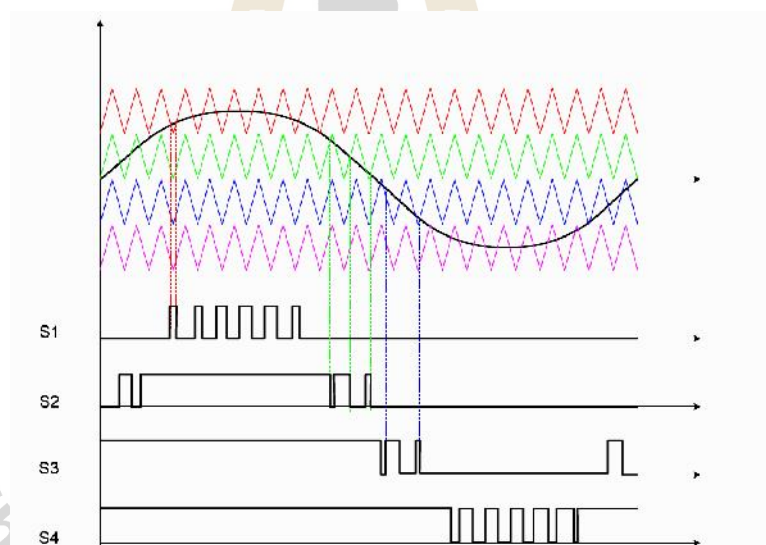


Figure 2.16 Phase Disposition SPWM

The methods that work with low switching frequencies generally perform one or two commutations of the power semiconductors during one cycle of the output voltages, the first generation of this method is the square wave two or three level converters, For multilevel converters, this techniques is the prepared the

switching angles by calculated for generating a staircase waveform. Representatives of this family are the multilevel selective harmonic elimination (SHE) (Li, L., Czarkowski, D., Liu, Y., and Pillay, P. 1998) and the space-vector control (SVC) (Rodríguez, J., Morán, L, Silva, C., and Correa, P., 2000).

2.5.2 Commutation Failure

Commutation failure can occur due to different behaviors and stability of voltage or power based on different features of the single-infeed HVDC system (Aik, D.L.H., and Anderson, G., 1997), it is an unavoidable problem in any type of DC power transmission system using thyristors. The commutation failure causes many problems to the valves, the reactive power of HVDC systems as well as the operation of the protective relays and so on. So, it should be investigated thoroughly before the system is designed. A thyristor is a device that has a turn-on capability, but no turn-off capability. The only way to turn it off is to apply a reverse signal to it (Aik, D.L.H., and Anderson, G., 2016). Recently, more researchers are interested in the commutation failure problems involving modeling and control, protection, analysis and mitigation. In the analysis, attractive areas are transient stability analysis and voltage and power stability analysis (Thio, C.V., Davies, J.B., and Kent, K.L., 1996).

2.5.3 Control of HVDC Transmission Systems

Traditional LCC-HVDC transmission system has played an important role in long distance bulk power transmission around the world since its first application. However some well-known limitations associated with it still exist today. One of the limitations is the reactive power requirement at both ends of the HVDC systems. In some researches this problem has been tackled by the application of controlled in-line capacitors. Recently a better solution has been developed which is

the use of VSC-HVDC systems. The VSC-HVDC systems offer many benefits compared to the conventional thyristor based approaches. Notable benefits of the VSC solution can be summarized as follows; The VSC controls both the amplitude and phase angle independently and rapid control of the active and reactive powers, The VSC does not depend on line-commutation, all four quadrants of the P-Q operating plane are possible and in VSC-HVDC control of the reactive power injection can achieve rapid voltage control at the converter bus, giving a strong dynamic enhancement to transient stability (Abbas, A.M., and Lehn, P.W., 2009).

Almost all LCC-based systems use some form of Current Margin Control (CMC). Coordinate Current Control (CCC) is the type of droop control and allows sending and receiving terminals to participate in current regulation to improve the dc link dynamics. Voltage Margin Control (VMC) is due to the CMC and is commonly used in VSC-based systems. AC Voltage Control (AVC) is used when one terminal is connected to a passive ac grid and the HVDC converter is responsible for regulating the ac voltage. More advanced control methods were usually developed as combination or extension of basic method (Shah, S., Hassan, R., and Sun, J., 2013).

Generally speaking, the control system of the VSC-HVDC is based on a fast inner current control loop and slower outer controllers, which supply the current references for the inner control loop (Fu, X., Dessaint, L.A., Gagnon, R., Zhou, K., and Cheng, M.A., 2012). For a normal operation of two terminals VSC-HVDC transmission, one VSC station will work in DC voltage and reactive power or AC voltage control mode, where VSC is used to maintain constant DC bus voltage and send required reactive power to its connected AC power network. On the other hand, the other VSC station will operated in active power and reactive power or AC voltage

control mode, where VSC is employed to regulate active and reactive power flow as required.

Due to the fact that MMC converter is the newest converter technology more researchers are interested in the modeling and control of both conventional Detail Model (DM) and Average-Valve Model (AVM) for simulating the MMC-based HVDC transmission systems (Xu, J., Gole, A.M., and Zhao, C., 2015). The control methods have different purposes, simulation program or application of their researches (Guan, M., and Xu, Z., 2012).

2.6 Conclusions

This paper has presented the review of HVDC transmission systems. The history and development of this technology has been explained in detail. The discovery of the mercury-arc valve has been presented. HVDC transmission systems can alleviate the problems of HVAC transmission systems. Step by step improvement of the HVDC transmission technology from mercury-arc valve based LLC-HVDC to the thyristor-based LCC-HVDC systems in 1970 is briefly outlined. This has been achieved due to the development of the power electronic switches. How the well-known limitations of LCC-HVDC were solved in mid 1990s when the voltage source converter was invented. The newest technology for HVDC that is VSC-HVDC systems is addressed. The thyristor-based LCC-HVDC systems and VSC-HVDC systems are suitable for applications depending on different purposed characteristic, power capacity and distance between the two systems. It has shown that HVDC configurations depend on the function and location of converter stations. The back-to-back HVDC system is part of this work. It is also expressed that in the Point-to-point

HVDC systems can either be monopolar or bipolar HVDC systems and for the multi-terminal HVDC systems there are more than two power converter stations connected. Several methods for controlling the firing angle of the thyristor for LCC-HVDC converter are explained. There are two methods that have been widely used, IPC and EPC. For VSC-HVDC converters, a very popular high switching frequency SPWM that has been widely used



CHAPTER V

MODELING AND CONTROL OF MMC-BASED HVDC TRANSMISSION SYSTEMS

5.1 Introduction

This chapter is present the modeling and control of modular multilevel converter (MMC) is applied to the high voltage direct current (HVDC) transmission system that transmission the power energy from the offshore wind farm to the onshore power systems. The modulation technique is proposed the particles swarm optimization (PSO) technique for minimized the total harmonic distortion (THD) and compared with conventional SPWM method. In this chapter show minimized THD by using PSO artificial intelligence search for switching angles for minimum THD and application to modular multilevel converter that connected with MMC-based HVDC transmission systems. The simulation results is compared the THD of conventional modulation method with proposed method.

The simulation systems of MMC-based HVDC transmission systems are improved from conventional VSC-HVDC systems by replaced the MMC converters to the conventional 3-level NPC converters. For the control systems of MMC-based HVDC systems are improved the modulation method for MMC and improve the control system in order suitable to MMC-based HVDC transmission systems. The simulation results that show the performance of control systems and compared the

THD between conventional SPWM method and proposed method

5.2 Modeling of VSC-HVDC Transmission Systems

The typical layout of point-to-point VSC-HVDC systems for power system integration of offshore wind farms is shown in Figure 5.1. The VSCs on the rectifier-side and inverter-side are consisting of self-commutated IGBTs to realize the AC/DC power transformation. The DC capacitors on both sides maintain the balance between the AC and DC power as the DC voltage sources. And the AC transformers and series reactors are connected to the AC buses on both sides of VSC-HVDC systems. And the high frequency filters (HHFs) are needed to eliminate the high frequency components of AC harmonics generated by module cell (Bahrman, M. P., and Johnson, B. K., 2007).

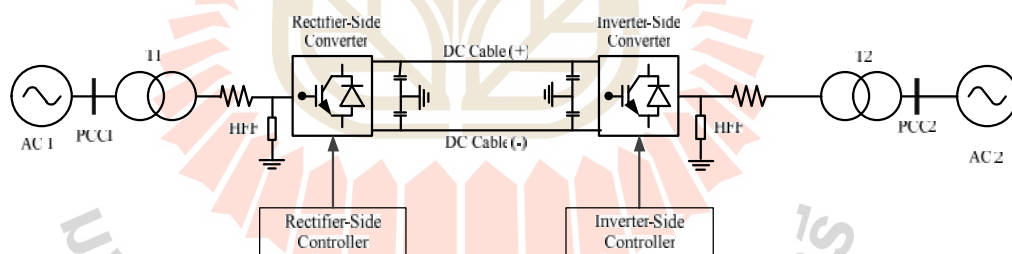


Figure 5.1 The General Configuration of Point-to-point VSC-HVDC System

5.2.1 Modeling of Rectifier-side Converter

The AC circuit on the rectifier-side converter in VSC-HVDC systems for power system integration of the offshore wind farm is shown in Figure 5.2. The relationship of three-phase voltages on the system-side and converter-side can be expressed by (4.1).

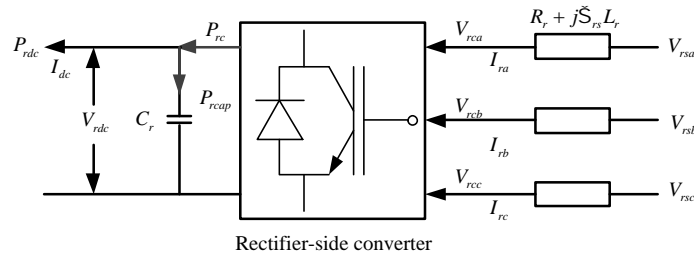


Figure 5.2 The Diagram of Rectifier-side Circuit

$$\begin{cases} V_{rsa} = V_{rca} + R_r I_{ra} + L_r \frac{dI_{ra}}{dt} \\ V_{rsb} = V_{rcb} + R_r I_{rb} + L_r \frac{dI_{rb}}{dt} \\ V_{rsc} = V_{rcc} + R_r I_{rc} + L_r \frac{dI_{rc}}{dt} \end{cases} \quad (5.1)$$

where V_{rsa} , V_{rsb} and V_{rsc} are the three-phase AC voltages at the PCC for external power system; V_{rca} , V_{rcb} and V_{rcc} are the three-phase AC voltages on the AC-side of rectifier; I_{ra} , I_{rb} and I_{rc} are the three-phase AC currents on the rectifier-side; L_r and R_r are the total inductance and resistance of the AC transformer and series AC reactor on the rectifier-side.

The (5.1) is converted from $a-b-c$ to $d-q$ coordinate system with the Park transformation matrix expressed in (5.2)

$$P_{rs} = \frac{2}{3} \begin{bmatrix} \cos(\check{S}_{rs}t) & \cos(\check{S}_{rs}t - \frac{2}{3}f) & \cos(\check{S}_{rs}t + \frac{2}{3}f) \\ -\sin(\check{S}_{rs}t) & -\sin(\check{S}_{rs}t - \frac{2}{3}f) & -\sin(\check{S}_{rs}t + \frac{2}{3}f) \end{bmatrix} \quad (5.2)$$

where P_{rs} is the rectifier-side Park transformation matrix; \check{S}_{rs} is the synchronous rotational speed of the AC system on the rectifier-side; $\check{S}_{rs} = 2f f_{rs}$ when f_{rs} is the system frequency on rectifier-side.

$$P_{rs} \begin{bmatrix} V_{rsa} \\ V_{rsb} \\ V_{rsc} \end{bmatrix} = P_{rs} \begin{bmatrix} V_{rca} \\ V_{rcb} \\ V_{rcc} \end{bmatrix} + R_r P_{rs} \begin{bmatrix} I_{ra} \\ I_{rb} \\ I_{rc} \end{bmatrix} + L_r P_{rs} \frac{d}{dt} \left(P_{rs}^{-1} P_{rs} \begin{bmatrix} I_{ra} \\ I_{rb} \\ I_{rc} \end{bmatrix} \right) \quad (5.3)$$

$$\begin{bmatrix} V_{rsd} \\ V_{rsq} \end{bmatrix} = \begin{bmatrix} V_{rcd} \\ V_{rcq} \end{bmatrix} + R_r \begin{bmatrix} I_{rd} \\ I_{rq} \end{bmatrix} + L_r P_{rs} P_{rs}^{-1} \begin{bmatrix} \frac{dI_{rd}}{dt} \\ \frac{dI_{rq}}{dt} \end{bmatrix} + P_{rs} \frac{dP_{rs}^{-1}}{dt} \begin{bmatrix} I_{rd} \\ I_{rq} \end{bmatrix} \quad (5.4)$$

$$P_{rs} \frac{dP_{rs}^{-1}}{dt} = \begin{bmatrix} 0 & -\check{S}_{rs} \\ \check{S}_{rs} & 0 \end{bmatrix} \quad (5.5)$$

After the transformation processes expressed from (5.3) to (5.5), the rectifier-side voltages in the rotating $d-q$ coordinate is expressed in (5.6)

$$\begin{cases} V_{rsd} = V_{rcd} + R_r I_{rd} + \frac{dI_{rd}}{dt} - \check{S}_{rs} L_r I_{rq} \\ V_{rsq} = V_{rcq} + R_r I_{rq} + \frac{dI_{rq}}{dt} + \check{S}_{rs} L_r I_{rd} \end{cases} \quad (5.6)$$

And the $d-q$ axis voltages on converter-side of rectifier-side converter are expressed by (5.7)

$$\begin{cases} V_{rcd} = V_{rsd} - R_r I_{rd} - \frac{dI_{rd}}{dt} + \check{S}_{rs} L_r I_{rq} \\ V_{rcq} = V_{rsq} - R_r I_{rq} - \frac{dI_{rq}}{dt} - \check{S}_{rs} L_r I_{rd} \end{cases} \quad (5.7)$$

where V_{rsd} and V_{rsq} are the $d-q$ axis voltage on the system-side of rectifier-side converter; V_{rcd} and V_{rcq} are the $d-q$ axis voltage on the converter-side of rectifier-

side converter; I_{rd} and I_{rq} are the $d-q$ axis currents of rectifier-side converter; $\tilde{\omega}_{rs}$ is the rotational angular speed of AC system on the rectifier-side.

So the dynamic models on the AC-side of the rectifier-side converter are given by Kalcon, et al (Kalcon, G. O., et al, 2012):

$$\begin{cases} \frac{dI_{rd}}{dt} = -\frac{R_r}{L_r} I_{rd} + \tilde{\omega}_{rs} I_{rq} + \frac{V_{rsd} - V_{rcd}}{L_r} \\ \frac{dI_{rq}}{dt} = -\frac{R_r}{L_r} I_{rq} - \tilde{\omega}_{rs} I_{rd} + \frac{V_{rsq} - V_{rcq}}{L_r} \end{cases} \quad (5.8)$$

The AC-side active power of the rectifiers is given by:

$$P_{rc} = V_{rcd} I_{rd} + V_{rcq} I_{rq} \quad (5.9)$$

Assuming the active power losses inside on the rectifier are neglected, there is the balance between the AC active power and DC power of the rectifier given by ((Kalcon, G. O., et al, 2012):

$$P_{rc} = P_{rcd} + P_{rcap} \quad (5.10)$$

$$V_{rcd} I_{rd} + V_{rcq} I_{rq} = V_{rdc} I_{rdc} + V_{rdc} C_r \frac{dV_{rdc}}{dt} \quad (5.11)$$

where P_{rc} is the active power on the rectifier-side; P_{rdc} is the DC power on the rectifier-side of DC cables; P_{rcap} is the power in the DC capacitor on rectifier-side and

C_r is the capacitance of DC capacitor; V_{rdc} and I_{rdc} are the voltage and current of the DC-side of converter on the rectifier-side.

So the dynamic equation for the DC voltage on rectifier-side is given by:

$$\frac{dV_{rdc}}{dt} = \frac{(V_{rcd}I_{rd} + V_{rcq}I_{rq})}{V_{rdc}C_r} - \frac{I_{rdc}}{C_r} \quad (5.12)$$

5.2.2 Modeling of Inverter-side Converter

The AC circuit on the inverter-side converter in VSC-HVDC systems for power system integration of the offshore wind farm is shown in Figure 5.3. The relationship of three-phase voltages on the system-side and inverter-side are defined as same as those on the rectifier-side.

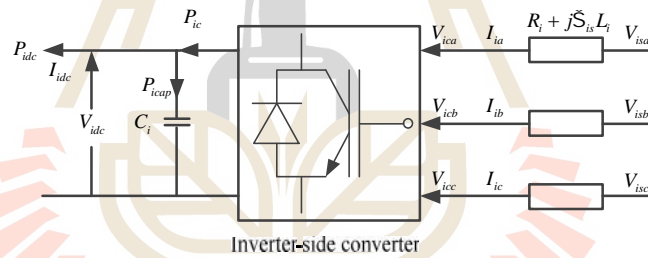


Figure 5.3 The Diagram of Inverter-side Circuit

$$\begin{cases} V_{isa} = V_{ica} + R_i I_{ia} + L_i \frac{dI_{ia}}{dt} \\ V_{isb} = V_{icb} + R_i I_{ib} + L_i \frac{dI_{ib}}{dt} \\ V_{isc} = V_{icc} + R_i I_{ic} + L_i \frac{dI_{ic}}{dt} \end{cases} \quad (5.13)$$

where V_{isa} , V_{isb} and V_{isc} are the three-phase AC voltages at the PCC for external power system on the inverter-side; V_{ica} , V_{icb} and V_{icc} are the three-phase AC voltages on the AC-side of inverter; I_{ia} , I_{ib} and I_{ic} are the three-phase AC currents on the inverter-

side; L_i and R_i are the total inductance and resistance of the AC transformer and series AC reactor on the inverter-side.

The (5.13) is converted from $a-b-c$ to $d-q$ coordinate system with the Park transformation matrix expressed in (5.14)

$$P_{is} = \frac{2}{3} \begin{bmatrix} \cos(\check{S}_{is}t) & \cos(\check{S}_{is}t - \frac{2}{3}f) & \cos(\check{S}_{is}t + \frac{2}{3}f) \\ -\sin(\check{S}_{is}t) & -\sin(\check{S}_{is}t - \frac{2}{3}f) & -\sin(\check{S}_{is}t + \frac{2}{3}f) \end{bmatrix} \quad (5.14)$$

where P_{is} is the inverter-side Park transformation matrix; \check{S}_{is} is the synchronous rotational speed of the AC system on the inverter-side; $\check{S}_{is} = 2f f_{is}$ when f_{is} is the system frequency on inverter-side.

$$P_{is} \begin{bmatrix} V_{isa} \\ V_{isb} \\ V_{isc} \end{bmatrix} = P_{is} \begin{bmatrix} V_{ica} \\ V_{icb} \\ V_{icc} \end{bmatrix} + R_i P_{is} \begin{bmatrix} I_{ia} \\ I_{ib} \\ I_{ic} \end{bmatrix} + L_i P_{is} \frac{d}{dt} \left(P_{is}^{-1} P_{is} \begin{bmatrix} I_{ia} \\ I_{ib} \\ I_{ic} \end{bmatrix} \right) \quad (5.15)$$

$$\begin{bmatrix} V_{isd} \\ V_{isq} \end{bmatrix} = \begin{bmatrix} V_{icd} \\ V_{icq} \end{bmatrix} + R_i \begin{bmatrix} I_{id} \\ I_{iq} \end{bmatrix} + L_i P_{is} P_{is}^{-1} \begin{bmatrix} \frac{dI_{id}}{dt} \\ \frac{dI_{iq}}{dt} \end{bmatrix} + P_{is} \frac{dP_{is}^{-1}}{dt} \begin{bmatrix} I_{id} \\ I_{iq} \end{bmatrix} \quad (5.16)$$

$$P_{is} \frac{dP_{is}^{-1}}{dt} = \begin{bmatrix} 0 & -\check{S}_{is} \\ \check{S}_{is} & 0 \end{bmatrix} \quad (5.17)$$

After the transformation processes expressed from (5.15) to (5.17), the inverter-side voltages in the rotating $d-q$ coordinate is expressed in (5.18)

$$\begin{cases} V_{isd} = V_{icd} + R_i I_{id} + \frac{dI_{id}}{dt} - \check{S}_{is} I_{iq} \\ V_{isq} = V_{icq} + R_i I_{iq} + \frac{dI_{iq}}{dt} + \check{S}_{is} I_{id} \end{cases} \quad (5.18)$$

And the $d-q$ axis voltages on converter-side of rectifier-side converter are expressed by (5.19)

$$\begin{cases} V_{icd} = V_{isd} - R_i I_{id} - L_i \frac{dI_{id}}{dt} + \check{S}_{is} L_i I_{iq} \\ V_{icq} = V_{isq} - R_i I_{iq} - L_i \frac{dI_{iq}}{dt} - \check{S}_{is} L_i I_{id} \end{cases} \quad (5.19)$$

where V_{isd} and V_{isq} are the $d-q$ axis voltage on the system-side of inverter-side converter; V_{icd} and V_{icq} are the $d-q$ axis voltage on the converter-side of inverter-side converter; I_{id} and I_{iq} are the $d-q$ axis currents of inverter-side converter; \check{S}_{is} is the rotational angular speed of AC system on the inverter-side.

So the dynamic models on the AC-side of the inverter-side converter are given by (Kalcon, G. O., et al, 2012):

$$\begin{cases} \frac{dI_{id}}{dt} = -\frac{R_i}{L_i} I_{id} + \check{S}_{is} I_{iq} + \frac{V_{isd} - V_{icd}}{L_i} \\ \frac{dI_{iq}}{dt} = -\frac{R_i}{L_i} I_{iq} - \check{S}_{is} I_{id} + \frac{V_{isq} - V_{icq}}{L_i} \end{cases} \quad (5.20)$$

Assuming the active power losses inside on the rectifier are neglected, there is the balance between the AC active power and DC power of the inverter given by Kalcon, et al (Kalcon, G. O., et al, 2012):

$$P_{ic} = P_{icd} + P_{icap} \quad (5.21)$$

$$V_{icd}I_{id} + V_{icq}I_{iq} = V_{idc}I_{idc} + V_{idc}C_i \frac{dV_{idc}}{dt} \quad (5.22)$$

where P_{ic} is the active power on the inverter-side; P_{idc} is the DC power on the inverter-side of DC cables; P_{icap} is the power losses of DC capacitor on rectifier-side and C_i is the capacitance of DC capacitor; V_{idc} and I_{idc} are the voltage and current of the DC-side of inverter-side. So the dynamic equation for the DC voltage on inverter-side is given by:

$$\frac{dV_{idc}}{dt} = \frac{(V_{icd}I_{id} + V_{icq}I_{iq})}{V_{idc}C_i} - \frac{I_{idc}}{C_i} \quad (5.23)$$

5.3 Control of Point-to-point VSC-HVDC System

5.3.1 The Rectifier-side VSC Controller

As described in section 5.2, the models of rectifier-side converter can be express by (5.7). So $L_r \frac{dI_{rd}}{dt}$ and $L_r \frac{dI_{rq}}{dt}$ are replaced from V_{rd}^* and V_{rq}^* using PI controllers expressed by (5.24)

$$\begin{cases} V_{rd}^* = L_r \frac{dI_{rd}}{dt} = K_{rp} (I_{rd}^{ref} - I_{rd}) + K_{ri} \int (I_{rd}^{ref} - I_{rd}) dt \\ V_{rq}^* = L_r \frac{dI_{rq}}{dt} = K_{rp} (I_{rq}^{ref} - I_{rq}) + K_{ri} \int (I_{rq}^{ref} - I_{rq}) dt \end{cases} \quad (5.24)$$

where I_{rd} and I_{rd}^{ref} are the d -axis current and its reference on the rectifier-side; I_{rq} and I_{rq}^{ref} are the q -axis current and its reference on the rectifier-side; K_{rp} and K_{ri} are the proportional and integral gains of PI controllers on the rectifier-side.

Assuming the ratio between the L_r and R_r is large enough, the R_r can be neglected and the (5.7) is expressed by (5.25)

$$\begin{cases} V_{rzd} = V_{rsd} - V_{rd}^* + \tilde{S}_{rs} L_r I_{rq} \\ V_{rzd} = V_{rsq} - V_{rq}^* - \tilde{S}_{rs} L_r I_{rd} \end{cases} \quad (5.25)$$

As similar to those controllers for power converters in wind turbines such as DFIGs and PMSGs, the two-stage are usually applied for power converters in the VSC-HVDC systems. For the outer controller on rectifier-side, the classic scheme 1 is usually used: the P Mode is usually applied to control the input active power at the PCC via the d -axis PI controller on the rectifier-side. For the Q Mode controlling the input reactive power at the PCC is usually used on the rectifier-side to maintain the voltage-level at PCC for grid integration of external power sources. So the equations for outer power controller on the rectifier-side are expressed by:

$$\begin{cases} I_{rd}^{ref} = K_{Pr} (P_r^{ref} - P_r) + K_{iPr} \int (P_r^{ref} - P_r) dt \\ I_{rq}^{ref} = K_{Qr} (Q_r^{ref} - Q_r) + K_{iQr} \int (Q_r^{ref} - Q_r) dt \end{cases} \quad (5.26)$$

where P_r and P_r^{ref} are the output active power and its reference on the rectifier-side PCC; Q_r and Q_r^{ref} are the output reactive power and its reference on the rectifier-side PCC; K_{Pr} and K_{iPr} are the proportional and integral gains of d -axis PI controller; K_{Qr} and K_{iQr} are the proportional and integral gains of q -axis PI controller.

According to (5.25) and (5.26), the diagram for the rectifier-side Inner Current Controller and Outer Power Controller of VSC-HVDC are illustrated in Figure 5.4

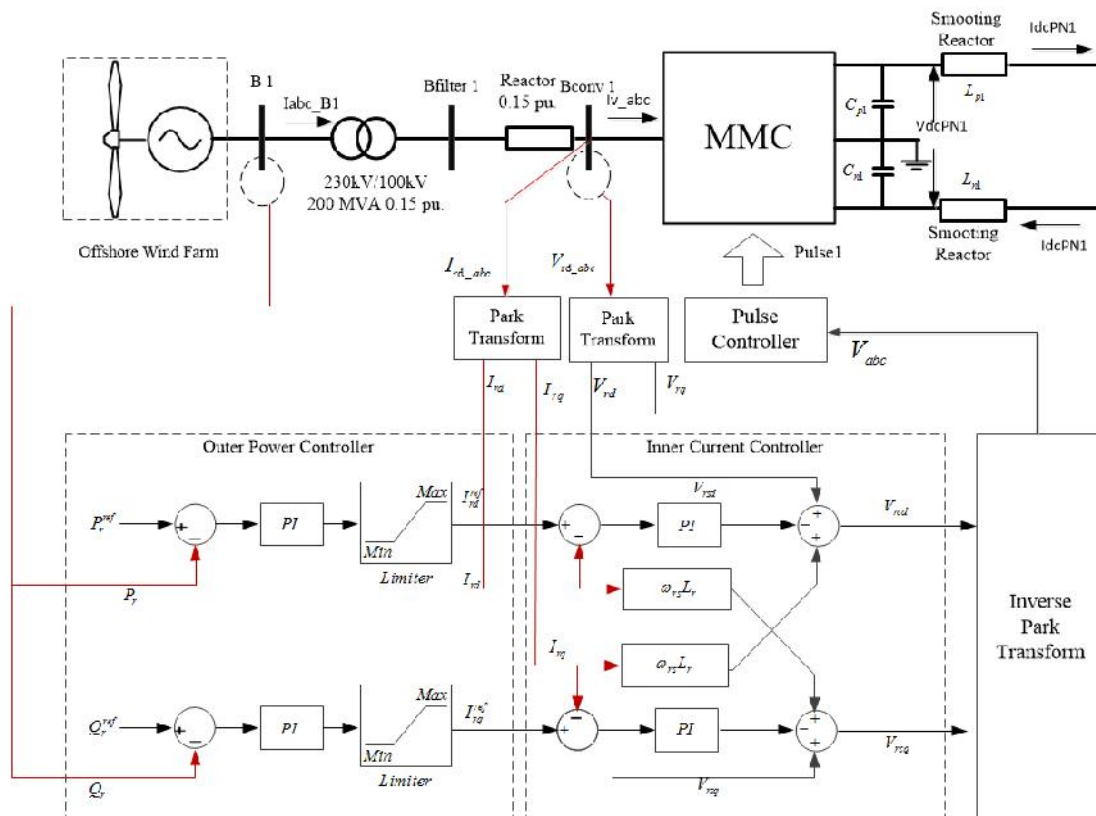


Figure 5.4 The Diagram for Outer Power Control of Rectifier-side VSC Controller

However, for the mainstream wind turbines such as WT-DFIGs, they

have equipped with the IGBT-based power converters and their output power can be controlled by their VSC controllers. So for the design of rectifier-side VSC controller, the scheme 2 can be applied for VSC controller which could just operate in q – axis V_{ac} Mode to provide the voltage reference at the PCC of rectifier-side for grid integration of offshore wind farms in synchronous operation. For the rotation d – q coordinate system rotates in synchronous with the one phase of the AC three-phase voltages at the synchronous speed \tilde{S}_s ($\tilde{S}_s = 2f f_s$), the d – q components of the AC voltages of the rectifier are given by (5.26). So (5.25) can be expressed by (5.27)

$$\begin{cases} V_{rd} = 0 \\ V_{rq} = V_{rc} \end{cases} \quad (5.27)$$

$$V_{rc} = V_{rsq} - V_{rq}^* - \tilde{S}_{rs} L_r I_{rd} \quad (5.28)$$

According to (5.28), the diagram for the rectifier-side Inner Current Controller in scheme 2 is illustrated in Figure 5.4. And the equation for outer q -axis V_{ac} controller on the rectifier-side is expressed by:

$$I_{rq}^{ref} = K_V (V_{rac}^{ref} - V_{rac}) + K_{iV} \int (V_{rac}^{ref} - V_{rac}) dt \quad (5.29)$$

where V_{rac} and V_{rac}^{ref} are the terminal AC voltage and its reference at PCC; K_V and K_{iV} are the proportional and integral gains of q -axis PI controller.

5.3.2 The Inverter-side VSC Controller

In the (5.19), the $L_i \frac{dI_{id}}{dt}$ and $L_i \frac{dI_{iq}}{dt}$ are replaced from V_{rd}^* and V_{rq}^*

using PI controller expressed by (5.30)

$$\begin{cases} V_{id}^* = L_i \frac{dI_{id}}{dt} = K_{ip} (I_{id}^{ref} - I_{id}) + K_{ii} \int (I_{id}^{ref} - I_{id}) dt \\ V_{iq}^* = L_i \frac{dI_{iq}}{dt} = K_{ip} (I_{iq}^{ref} - I_{iq}) + K_{ii} \int (I_{iq}^{ref} - I_{iq}) dt \end{cases} \quad (5.30)$$

where I_{id} and I_{id}^{ref} are the d -axis current and its reference on the inverter-side;

I_{iq} and I_{iq}^{ref} are the q -axis current and its reference on the inverter-side; K_{ip} and

K_{ii} are the proportional and integral gains of PI controllers of the current controller

on the inverter-side. Assuming the ratio between the L_i and R_i is large enough, the R_i can be neglected and the (5.19) is expressed by (5.31)

$$\begin{cases} V_{icd} = V_{isd} - V_{id}^* + \tilde{S}_{is} L_i I_{iq} \\ V_{icq} = V_{isq} - V_{iq}^* - \tilde{S}_{is} L_i I_{id} \end{cases} \quad (4.38)$$

According to (5.31), the diagram for the inverter-side VSC controller is illustrated in the Figure 5.5

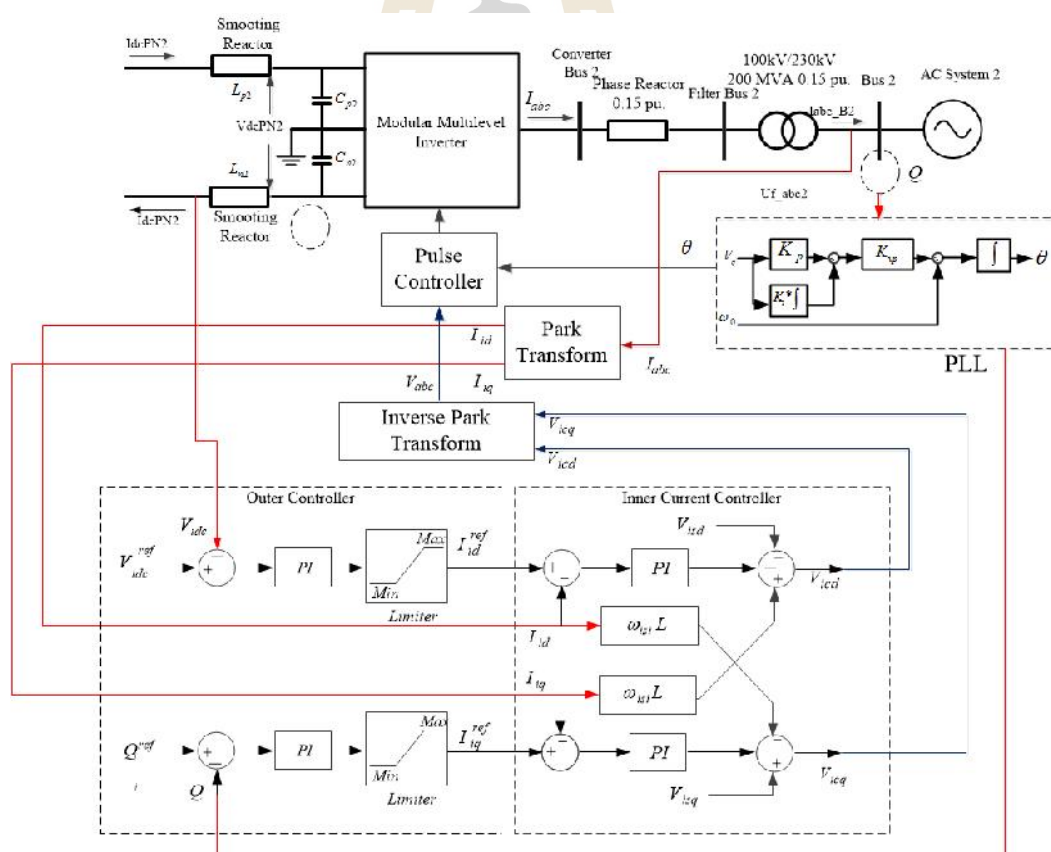


Figure 5.5. The Diagram of Inverter-side VSC Controller

For the first-stage *PI* regulator in *d* – axis , the V_{dc} Mode is applied for maintaining the DC voltage for AC/DC power transformation. For the *q* – axis *PI* regulator, the *Q* Mode is applied to control the output reactive power into the external power system. So the equations for outer controller on the inverter-side are expressed by:

$$\begin{cases} I_{id}^{ref} = K_{dc}(V_{idc}^{ref} - V_{idc}) + K_{idc} \int (V_{idc}^{ref} - V_{idc}) dt \\ I_{iq}^{ref} = K_{Qi}(Q_i^{ref} - Q_i) + K_{iQi} \int (Q_i^{ref} - Q_i) dt \end{cases} \quad (5.32)$$

where V_{idc} and V_{idc}^{ref} are the DC voltage and its reference of the inverter-side converter; Q_i and Q_i^{ref} are the output reactive power and its reference on the inverter-side PCC; K_{dc} and K_{idc} are the proportional and integral gains of *d* – axis *PI* controller; K_{Qi} and K_{iQi} are the proportional and integral gains of *q* – axis *PI* controller.

5.4 Simulation of MMC-Based VSC-HVDC Transmission Systems

5.4.1 System Configurations

This case study is presented about 200 MVA MMC-based VSC-HVDC interconnection is used to transmit power from the offshore wind farm 230 kV, 200 MVA, 50 Hz system to another identical AC system. The modeling of offshore wind farm is present in the previous section, and the configuration is shown in Figure 5.1 and the simulation system configuration is shown in Figure 5.7

The discrete control systems is compared the total harmonic distortion of sinusoidal modulating signals that are the reference value of the bridge phase voltages and particle swarm optimized total harmonic distortion method. The amplitude and phase of the modulating signals can be calculated to control either, the

reactive and real AC power flow at the PCC, or the reactive power flow at the PCC and the pole to pole DC voltage. It would also be possible to control the AC voltage amplitude at the PCC.

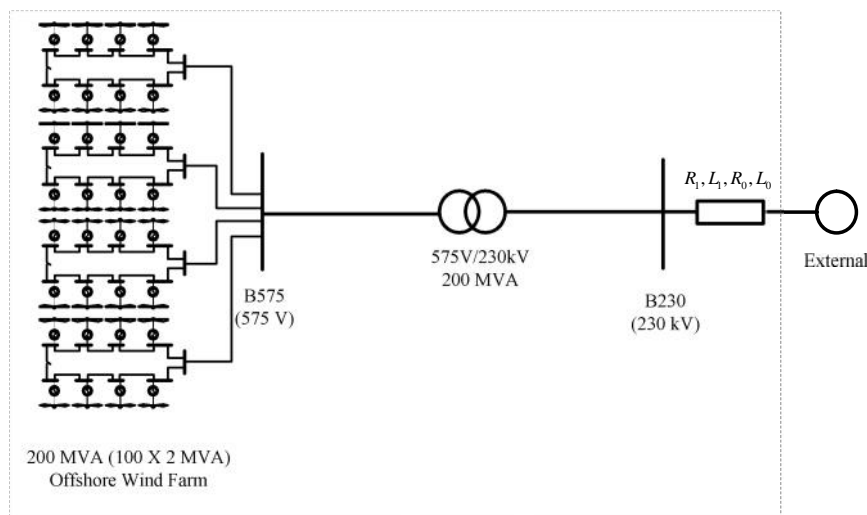


Figure 5.6 The Diagram of Offshore Wind Farm

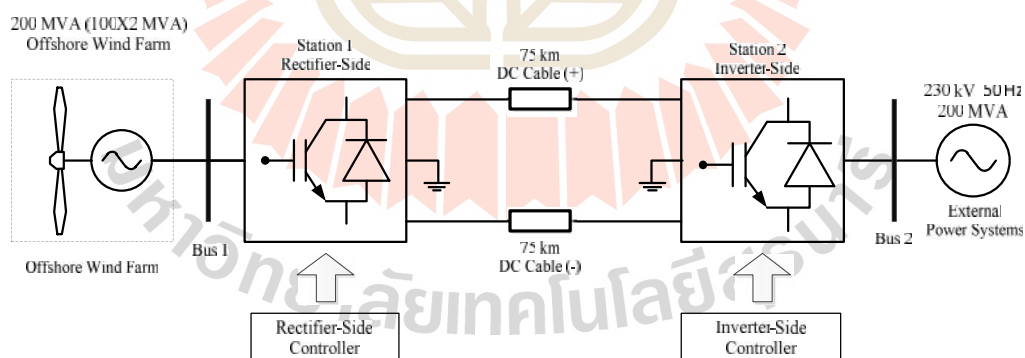


Figure 5.7 The Diagram of 3-level VSC-HVDC Offshore Wind Farm

The inverter side control for MMC-based VSC-HVDC is proposed is shown in Figure 5.8, the method calculates a voltages time area across the equivalent

reactor L which is required to change the current from present value to the reference value. The vector control operates in the synchronous rotating $dq0$ -frame and its main components are the phase-lock-loop (PLL), inner and outer control blocks. The inner controller regulates the converter ac voltage that will be used to generate the modulated switching pattern and the outer controller regulates the current reference needed to control the main VSC parameters such as power flow, ac voltage and dc voltage. Using vector control, the active and reactive power can be independently controlled by regulating current in the $dq0$ -frame.

When a VSC terminal is connected to an active ac system, the frequency and phase must be detected at a pre-defined reference point in order to synchronize the converter and control system accordingly. This action is performed by the PLL circuit which synchronizes a local oscillator with a sinusoidal reference input coming from the system's ac voltage. This ensures that the local oscillator is at the same frequency and in phase with the reference voltage input. The local oscillator is a voltage controller oscillator (VCO). The block diagram of the PLL is shown in Figure 5.9, where V_q is the q -axis voltage coming from the $abc-dq0$ transformation of the voltage reference and \tilde{S}_0 is a base system frequency. The component V_q is selected as it is proportional to $\sin(\theta)$ and $\sin(\theta) \approx \theta$ for small values of the angle θ . When the converter is connected to a passive system, such as a load connection or a wind farm, the frequency is fixed to \tilde{S}_0 by the PLL and only the frequency oscillator is required to generate the angle θ . This control approach will be used to implement a voltage/frequency VSC controller for system integrating offshore wind generation.

The other control, Outer control and Inner current control systems and block diagrams are shown in section 5.2.

Figure 5.10 is shown voltage and current are measured for pulse control in simulation program and Figure 5.11 is shown inside the pulse 2 controller, The PLL, outer control and inner current control are included in the VSC-Controller.

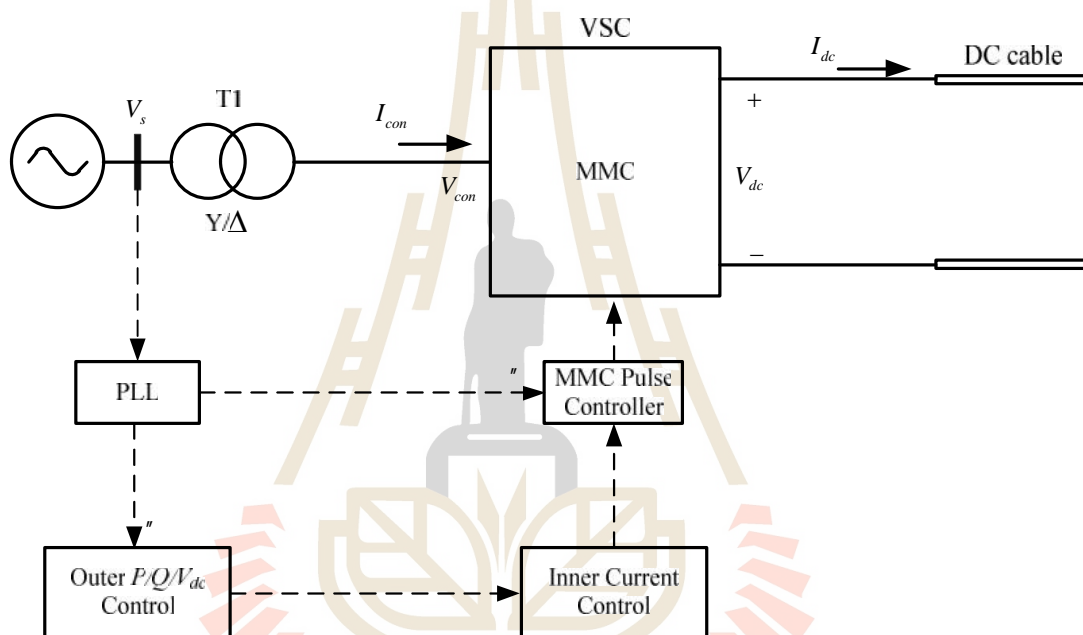


Figure 5.8 The MMC based VSC diagram

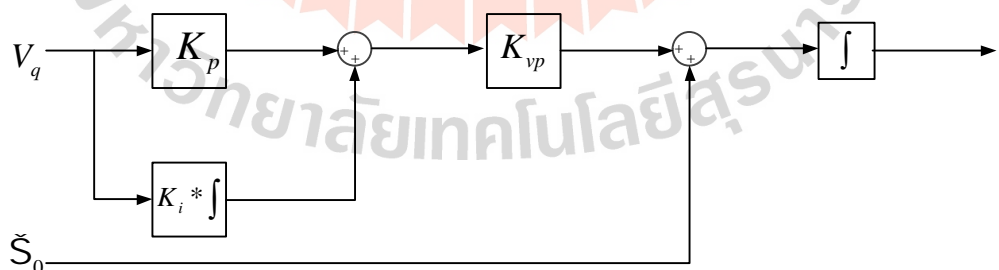


Figure 5.9 Phase-lock-loop block diagram

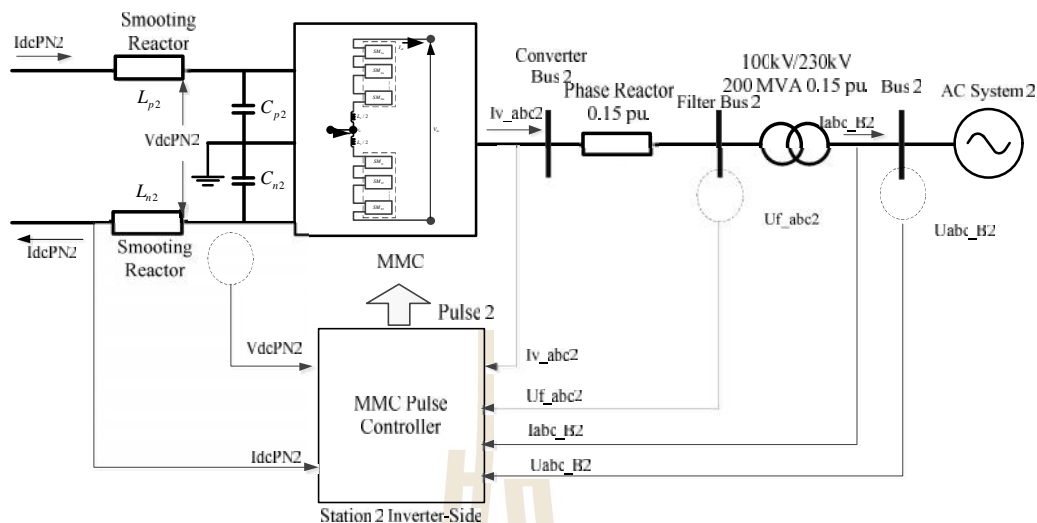


Figure 5.10 The measured points and control systems

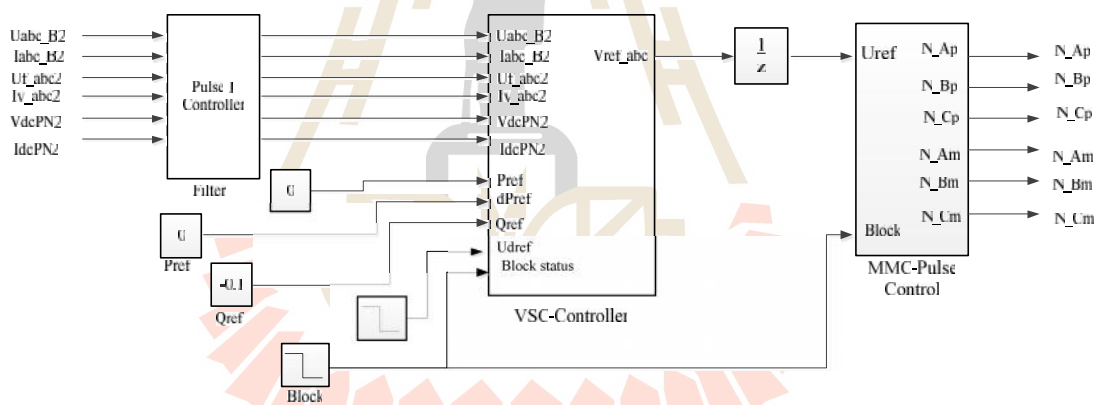


Figure 5.11 MMC pulse controller

5.4.2 Modulation Techniques

This section is proposed the both modulation techniques for MMC pulse controller. First, the Carrier-Shift SPWM is applied to modulate the modular multilevel converters. And then the optimized harmonic is applied. The simulations

are compared between the both modulation technique and conventional three-level VSC-HVDC transmission systems.

5.4.2.1 Carrier-Shift SPWM

The Carrier-Shift SPWM is shown in Figure 5.12. From above, the control schemes are presented. The VSC controller is the control system of the inverter side controller, the output of the VSC controller is the three phase reference voltage. Therefore, their three phase reference voltage is the input for the MMC pulse controller block. The Carrier-Shift SPWM modulation method, a number of N_c - cascaded cells in one phase with their carriers shifted by an angle $\mu_c = 360^\circ/N_c$ and using the same control voltage produce a load voltage with the smallest distortion. This result has been obtained for the multi-cell inverter in a seven-level configuration, which uses three series-connected cells in each phase. The smallest distortion is obtained when the carriers are shifted by an angle of $\mu_c = 360^\circ/3 = 120^\circ$.

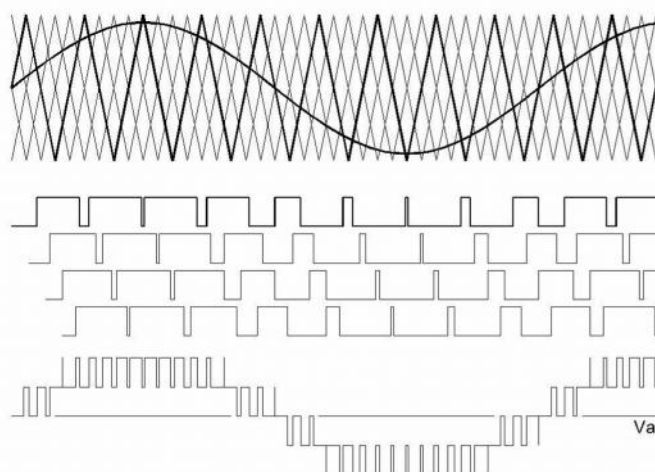


Figure 5.12 The Carrier-Shift SPWM

5.4.2.2 Optimized Harmonic Stepped Waveform (OHSW)

The Optimized Harmonic Stepped Waveform (OHSW) technique is non-carrier base PWM techniques are present in last chapter. It can be used for minimized harmonic distortion for calculated switching angle in the first quarter cycle can be considered variables for optimization. This research is proposed the PSO for calculated the switching angles, and minimum the total voltage harmonic distortion (THD) is presented above. The MMC pulse control block of this method, the MMC pulse control block had received the three phase reference voltage from VSC controller block, their reference voltage is compared with the switching angles are calculated for any step of modular multilevel inverter.

5.5 Simulation Results

5.5.1 Simulation Results of Rectifier Side

The simulation is started from 0 pu., at the time, $t = 0.3$ seconds is increased to 1.0 pu., at the time, $t = 1$ seconds. The system is three phase fault at the time, $t = 1.5$ seconds and fault is cleared at the time, $t = 1.55$ seconds. The simulation results of rectifier side on measurement bus (bus 1), the active power and its referent are shown in Figure 5.13. The reactive power referent is set equal 1.0 pu and step-down to -0.1 pu. at the time, $t = 2.0$ seconds. The simulation results of the reactive and reactive power referent on measurement bus (bus 1) are shown in Figure 5.14. The three phase voltage and current characteristic are shown in Figure 5.15 and 5.16 respectively.

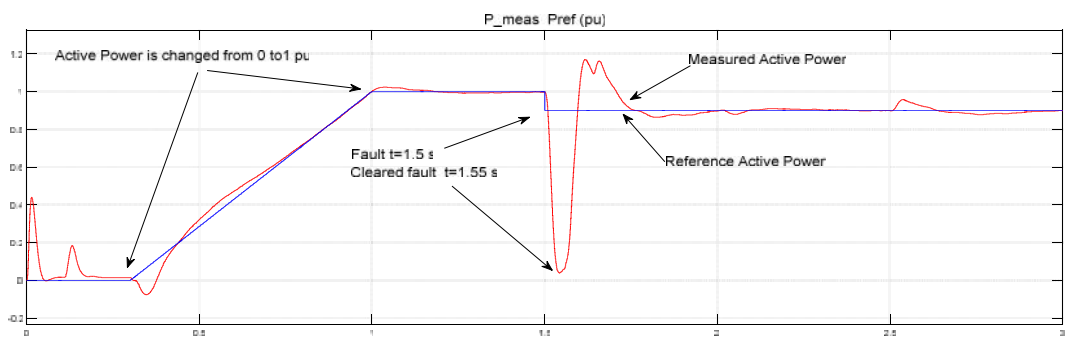


Figure 5.13 The measured active power and its referent on bus 1

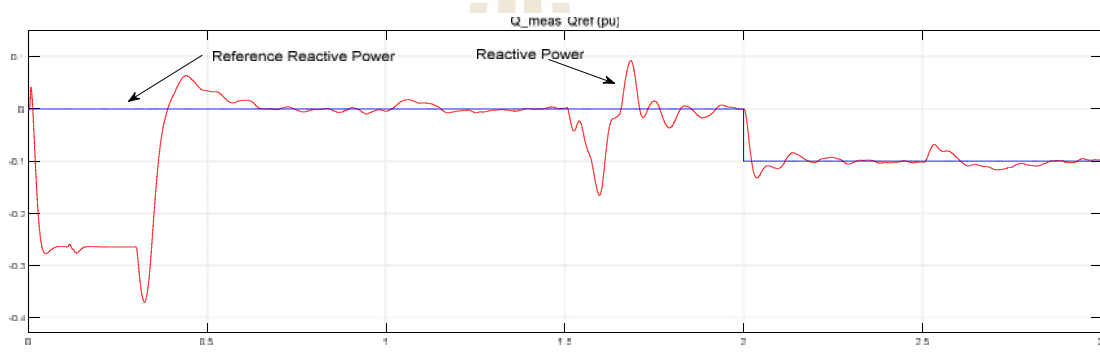


Figure 5.14 The measured reactive power and its referent on bus 1

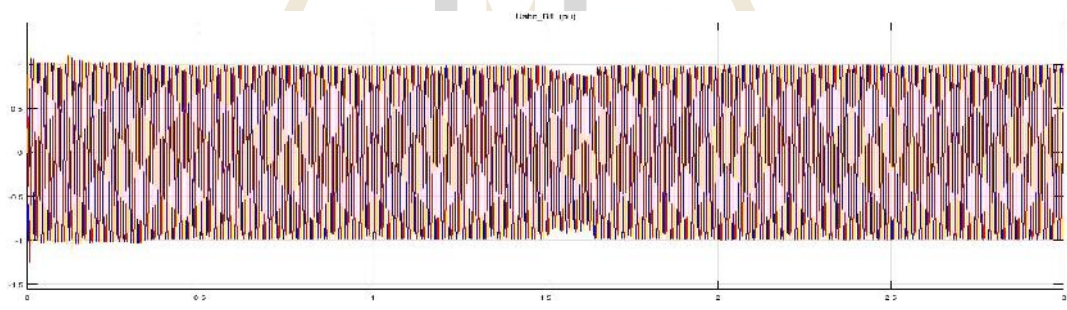


Figure 5.15 The measured voltage on bus 1

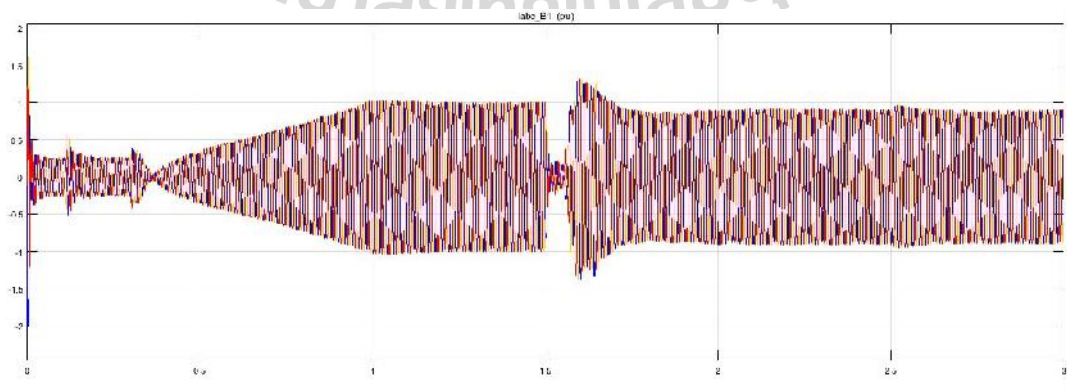


Figure 5.16 The measured current on bus 1

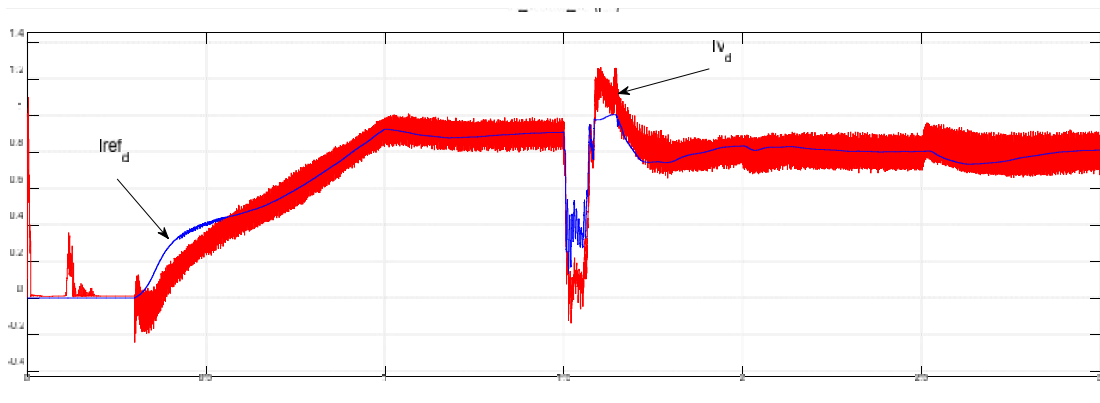


Figure 5.17 The measured d – axis control current and its referent on bus 1

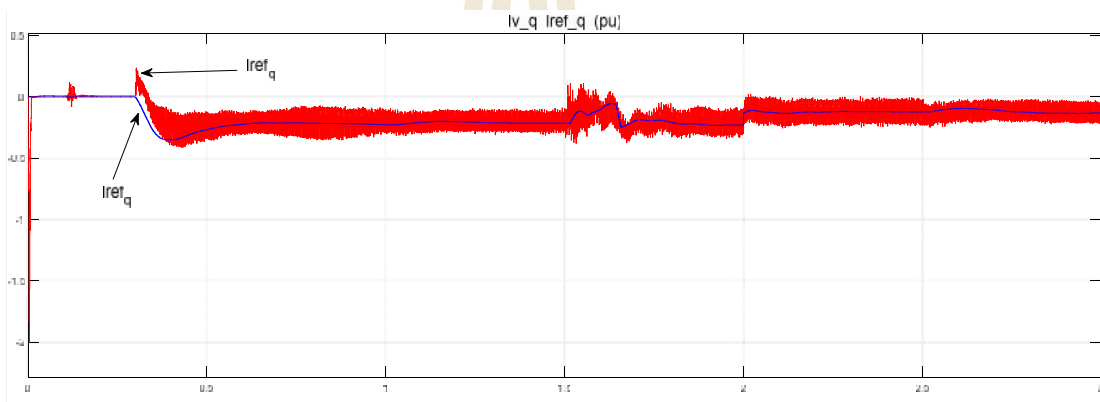


Figure 5.18 The measured q – axis control current and its referent on bus 1

The Figure 5.17 is shown the current is measured on the bus 1 is compared with the its referent current on d – axis and the Figure 5.18 are shown the current is measured on the bus 1 is compared with the its referent current on q – axis

5.5.2 Simulation Results of DC Bus

The simulation result of dc voltage on dc bus is shown in Figure 5.20 and the Figure 5.21 is shown the DC actual voltage and DC referent that set to 1.0 pu. The dc power is shown in Figure 5.22.

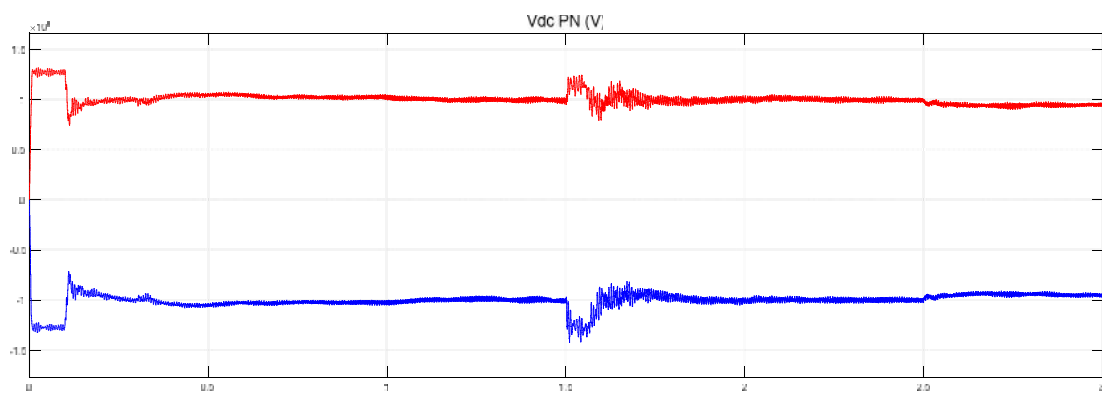


Figure 5.20 Simulation results; DC voltages

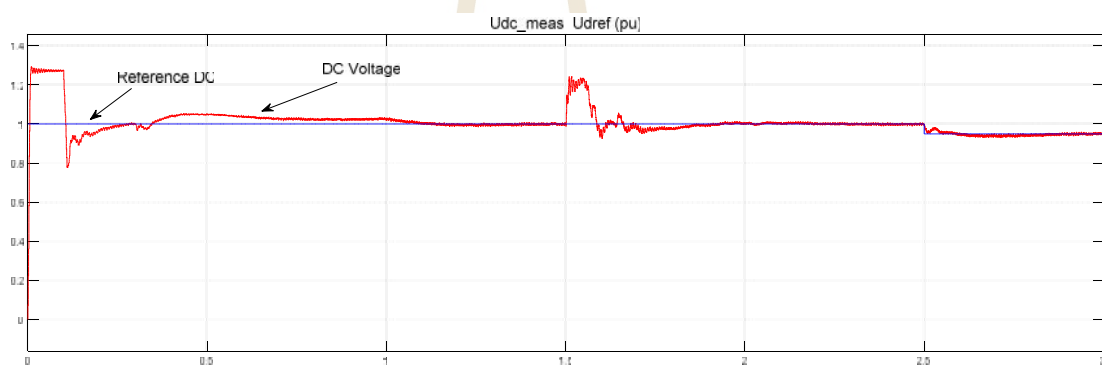


Figure 5.21 The measured DC voltages and its referent

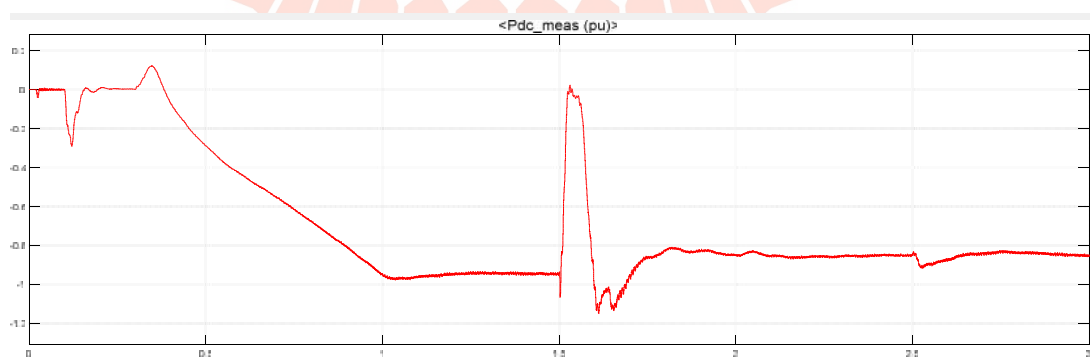


Figure 5.22 The measured DC power

5.5.3 Simulation Results of Inverter Side

The simulation results of the inverter side station, the referent current control and actual current on d -axis and q -axis are shown in Figure 5.23 and 5.24 respectively.

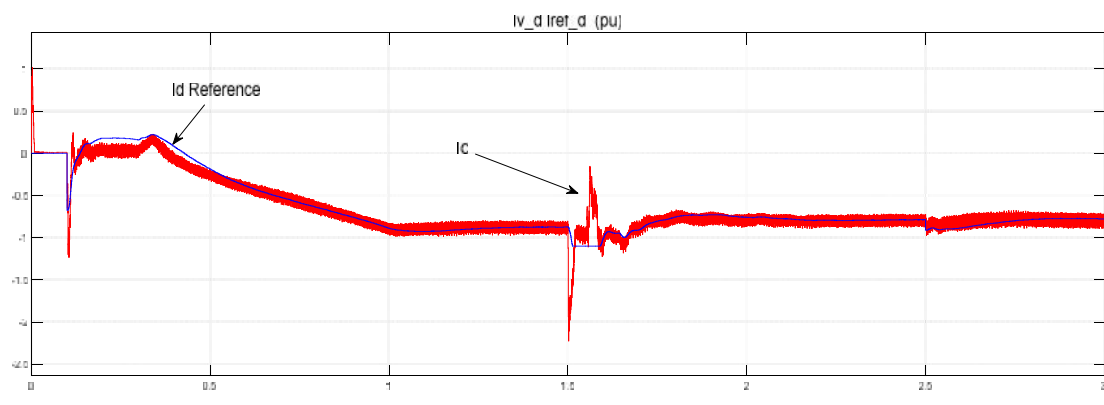


Figure 5.23 The measured d -axis control current and its referent on bus 2

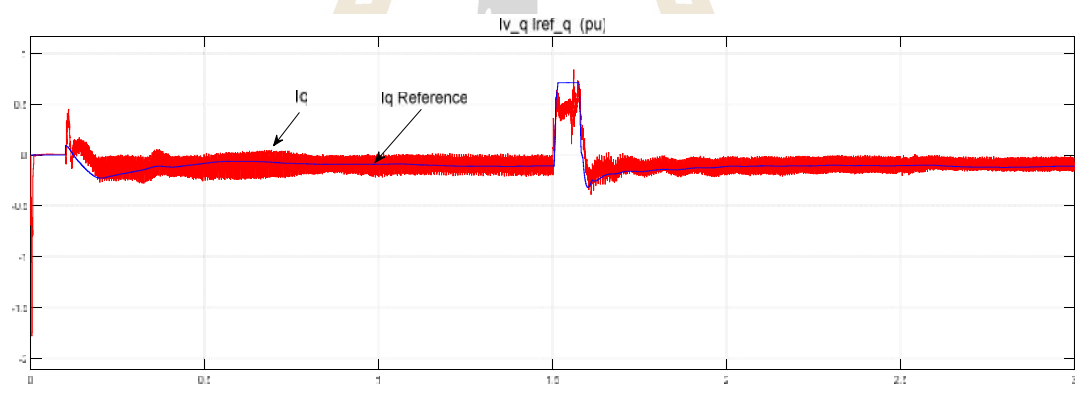


Figure 5.24 The measured q -axis control voltage and its referent on converter bus 2

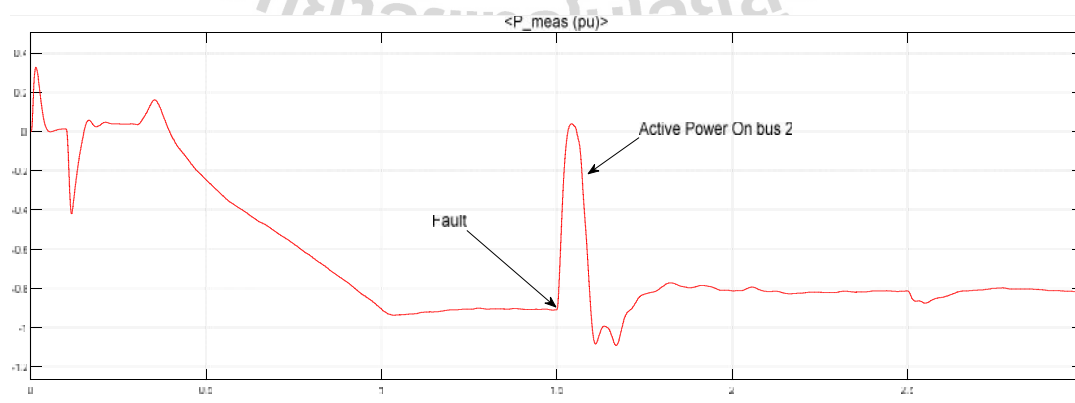


Figure 5.25 The active power on bus 2

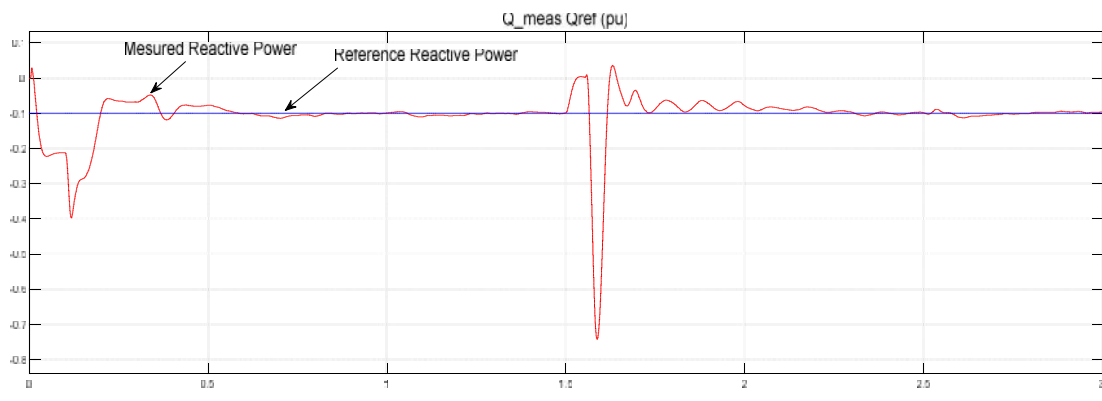


Figure 5.26 The measure reactive power and its referent on bus 2

The simulation result of active power on bus 2 is shown in Figure 5.25, and the measured power is compared with its referent reactive power on bus 2 is shown in Figure 5.26. The three phase voltage and current characteristic are shown in Figure 5.27 and 5.28 respectively.

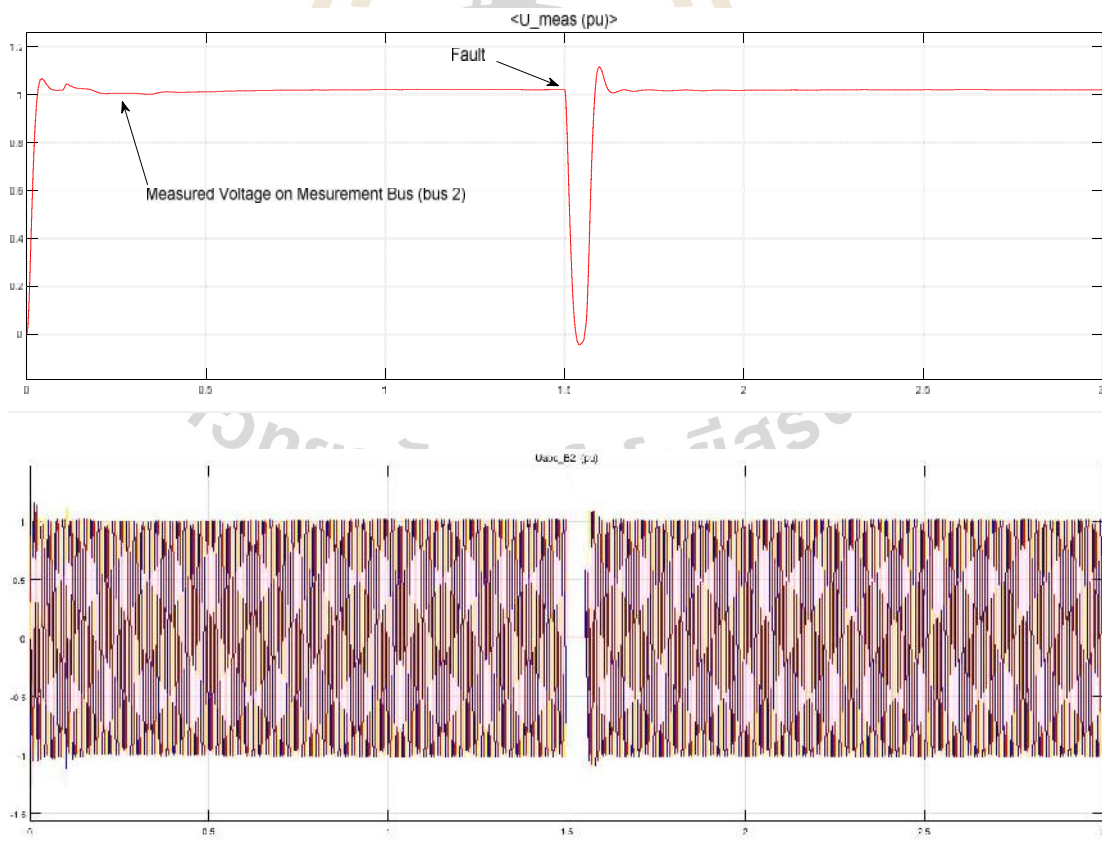


Figure 5.27 The voltage characteristic on bus 2

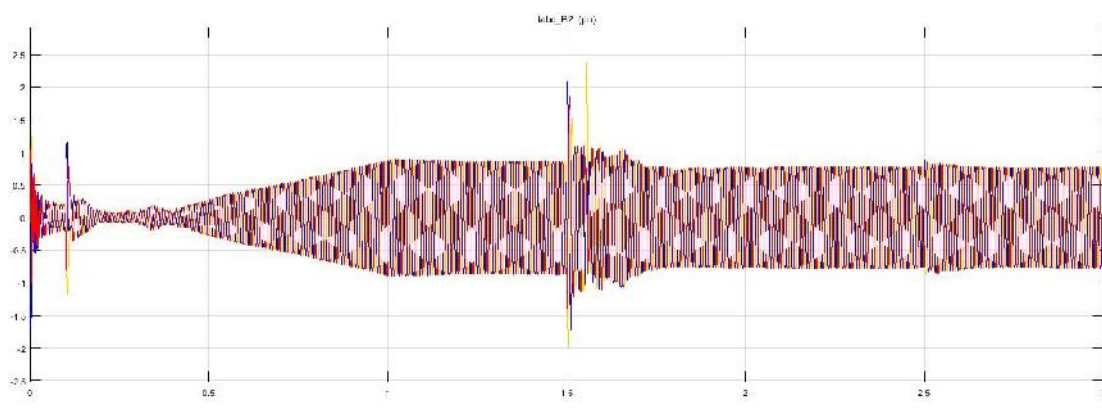


Figure 5.28 The current characteristic on bus 2

5.5.4 Simulation Results of MMC-Based HVDC Systems

The simulation results of the 73 level MMC-based VSC-HVDC, the output voltage are generated by the MMC is nearly sinusoidal are shown in Figure 5.29, therefore is not required output filters, if compared in 3-level VSC-HVDC transmission system. The inverter output voltage is filtered by the inductance phase reactor and inductance in the transformer, therefore the voltage at the PCC point bus 2 is sinusoidal by not required filtering are shown in Figure 5.30.

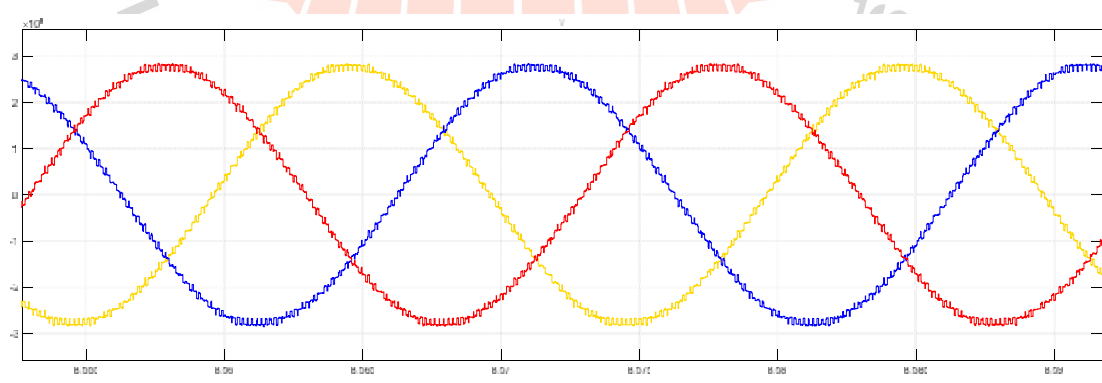


Figure 5.29 The AC voltage waveform for 73-level MMC

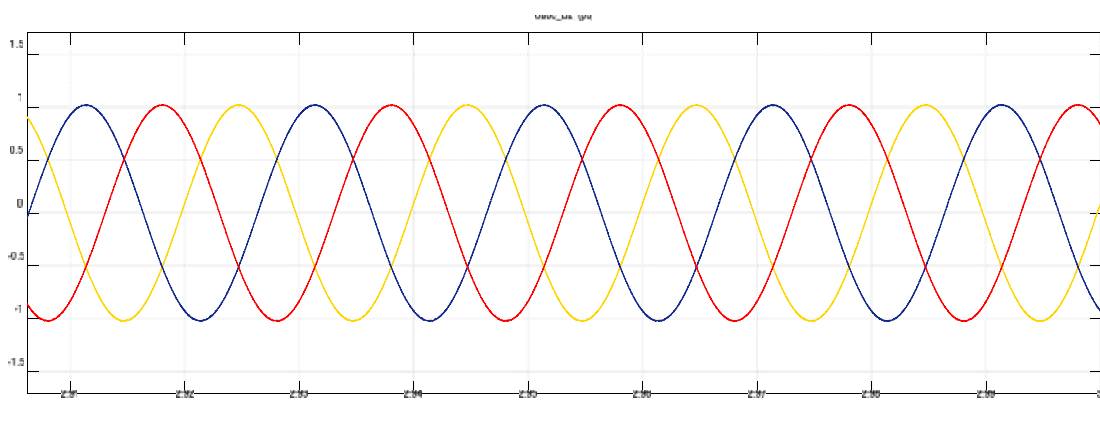


Figure 5.30 The AC voltage waveform of MMC-based HVDC at the Bus 2.

The simulation results, after the three phase is faulted at $t = 1.5$ seconds and cleared at $t = 1.55$ seconds, the voltage characteristics is shown in Figure 5.31. The simulation result of active power on bus 2 is shown in Figure 5.32, and the measured is compared with reference reactive power on bus 2 is shown in Figure 5.33. The Figure 5.34 and 5.35 are shown the three-phase voltage and current on bus 2, respectively.

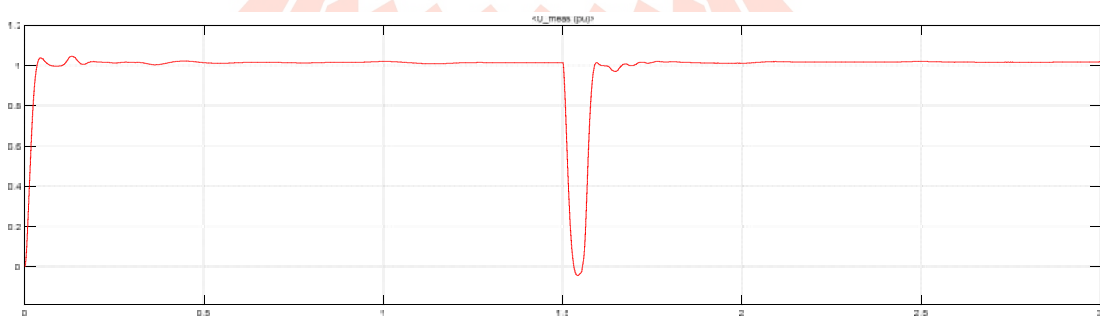


Figure 5.31 The AC voltage waveform of MMC-based on bus 2

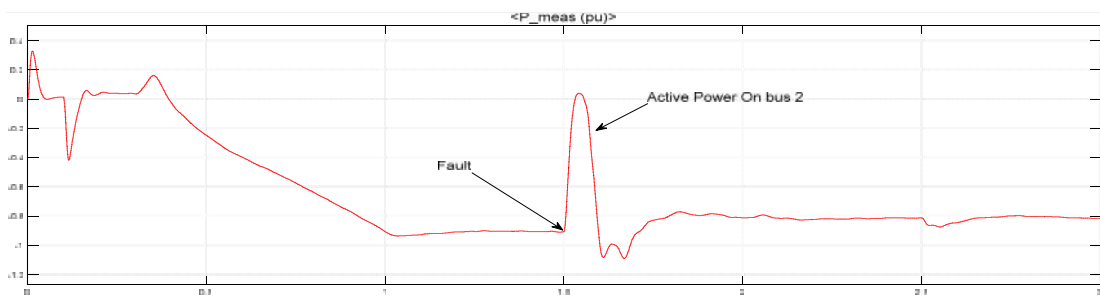


Figure 5.32 The active power on bus 2

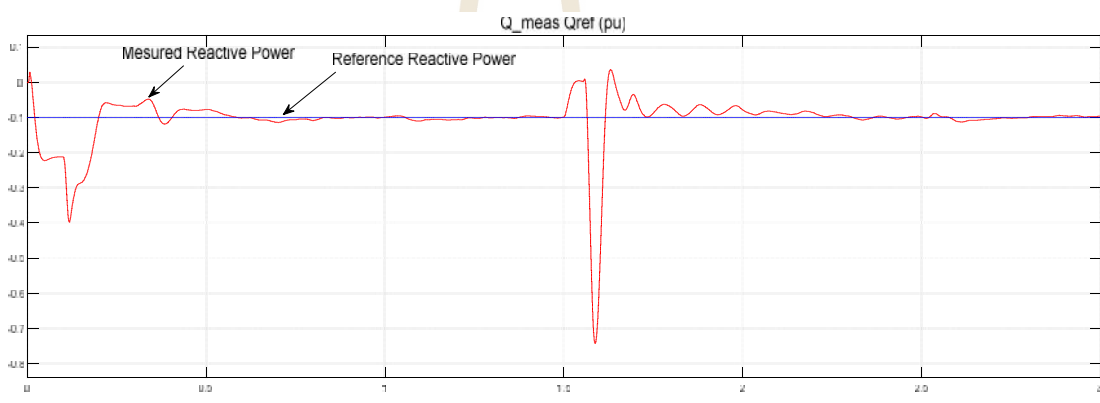


Figure 5.33 The measure reactive power and its referent on bus 2

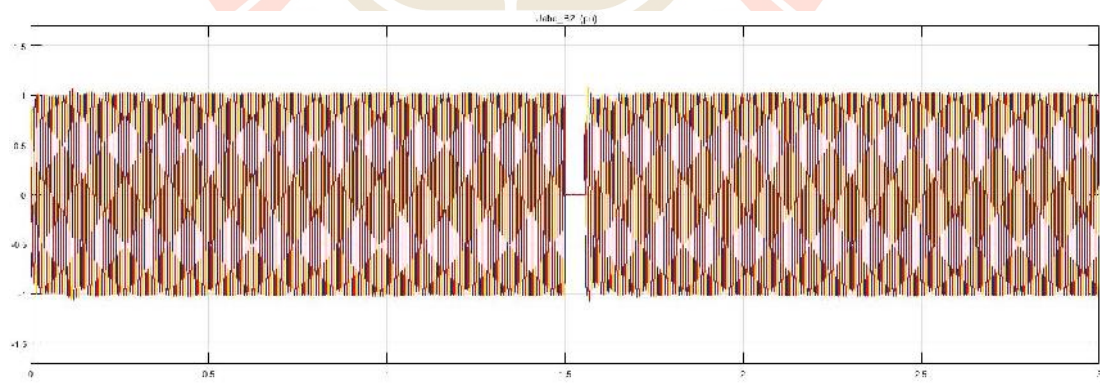


Figure 5.34 The three phase voltage characteristic on the Bus 2

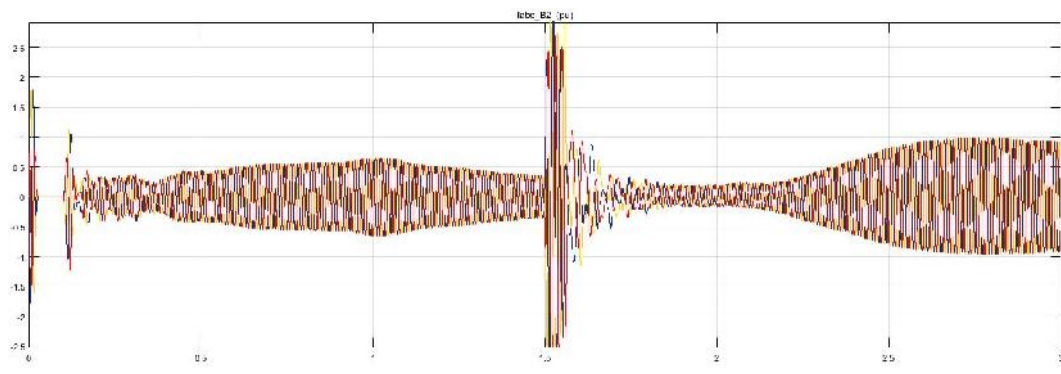


Figure 5.35 The three phase current characteristic on the Bus 2

The modulation technique is used high frequency carrier-shift SPWM, the carrier signals and reference signal are shown in Figure 5.36

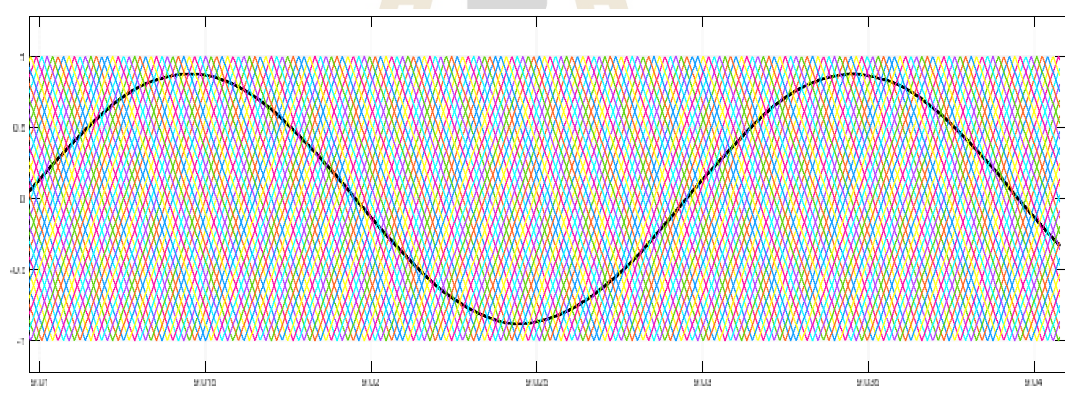


Figure 5.36 The modulation technique of Carrier-shifted SPWM

The simulation results of the OHSW 73 level MMC-based VSC-HVDC, the output voltage are generated by the MMC is nearly sinusoidal are shown in Figure 5.37, therefore is not required output filters, if compared in 3-level VSC-HVDC transmission system. The inverter output voltage is filtered by the inductance phase reactor and inductance in the transformer, therefore the voltage at the PCC point bus 2 is sinusoidal by not required filtering.

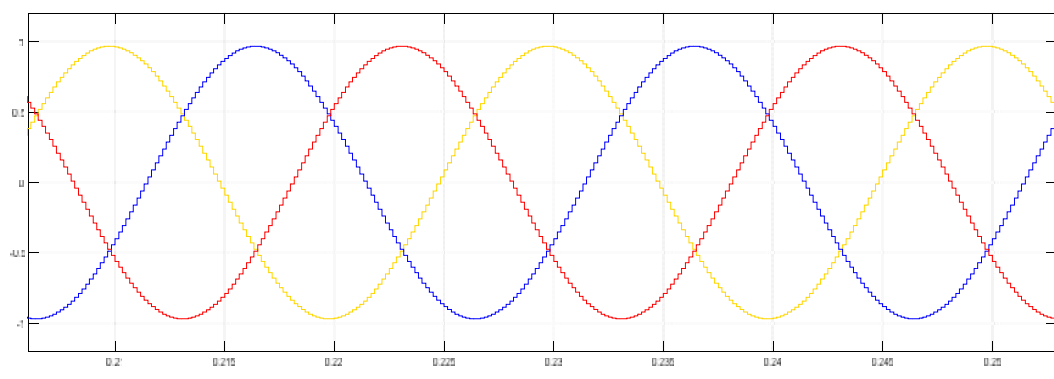


Figure 5.37 The AC voltage waveform of OHSW method for 73-level MMC-based VSC-HVDC transmission system

5.6 Harmonic Analysis

5.6.1 The Total Harmonic Distortion Requirements

The harmonic distortion is the one of biggest problems in power quality. Therefore, the IEEE is promoted the IEEE 519 standard, the IEEE 519-1981 is the first edition. Recently, third edition is IEEE 519-2014: IEEE Recommended Practice and Requirements for Harmonic Control in Electrical Power Systems. The limits in this recommended practice are intended for application at a point of common coupling (PCC). At PCC, system owners or operators should limit voltage harmonics as Table 5.1.

Table 5.1 Voltage distortion limits

Bus Voltage at PCC	Individual harmonic (%)	Total harmonic distortion THD (%)
$V < 1.0 \text{ kV}$	5.0	8.0
$1 \text{ kV} < V < 69 \text{ kV}$	3.0	5.0
$69 \text{ kV} < V < 161 \text{ kV}$	1.5	2.5
$161 \text{ kV} < V$	1.0	1.5*

Note * High voltage systems can behave up to 2.0% THD where the cause in an HVDC terminal whose effects will have attenuated at points in the network where future user may be connected.

5.6.2 Harmonic Analysis

This section will compare and analysis the harmonic that generated by HVDC converter and IEEE standard requirements. From simulation results of MMC-based HVDC systems are compared with conventional 3-level VSC-HVDC systems. The output voltage THD of conventional three-level VSC is measured at the converter bus station is 73.2 % is shown in Figure 5.38 and compared with the out voltage THD of 9-level MMC-based HVDC system is measured on converter bus is 21.5% that shown in Figure 5.38 and 5.39 respectively.

The simulation results are shown the individual harmonic and THD of output voltage waveforms are required the output filters because over the IEEE standards requirement.

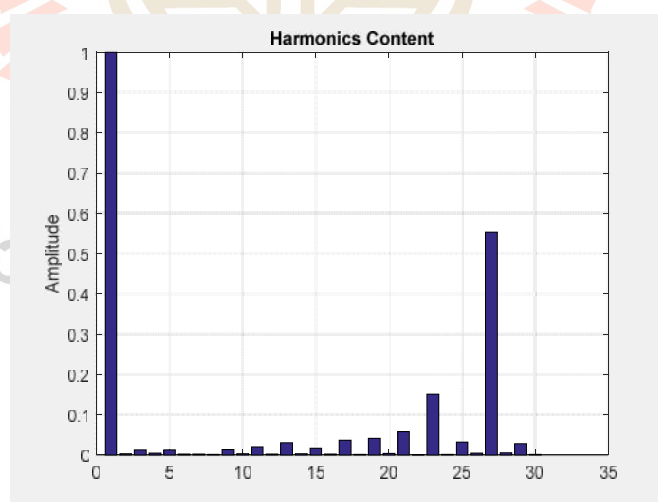


Figure 5.38 The harmonic distortion of 3-level VSC is modulated PWM method, THD=73.2%

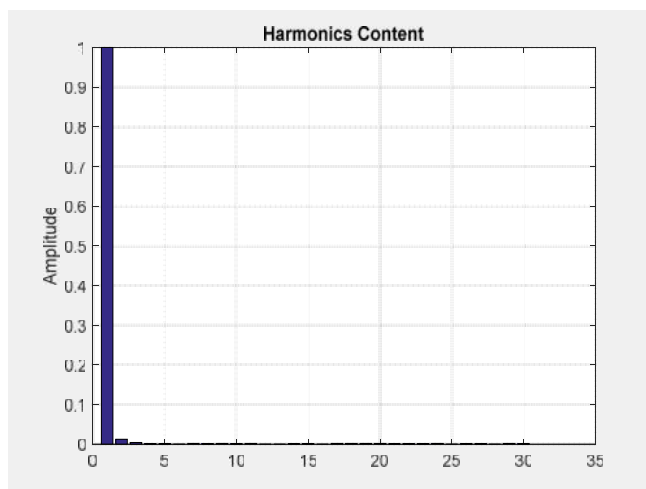


Figure 5.39 The phase to phase voltage harmonic is measured of 9-level MMC inverter is modulated by Carrier-shifted SPWM, the THD = 21.5%

The simulation results of the line-to-neutral and line-to-line voltage waveform of 11-level MMC inverter is modulated by the Carrier-shifted SPWM method are shown in Figure 5.40 and 5.41, respectively. The harmonic content of line-to-line voltage is shown in Figure 5.42. From simulation results that shown, the small output filters is required.

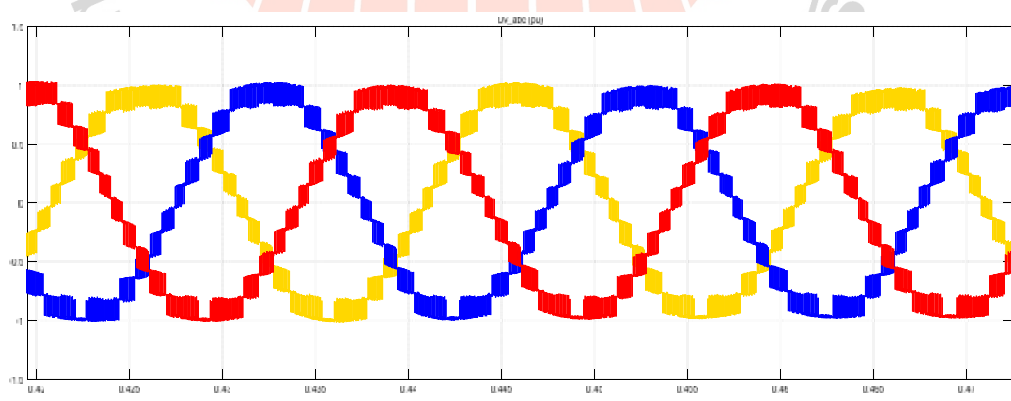


Figure 5.40 The three phase line-to-neutral output voltage of 11-level MMC inverter is modulated by Carrier-shifted SPWM

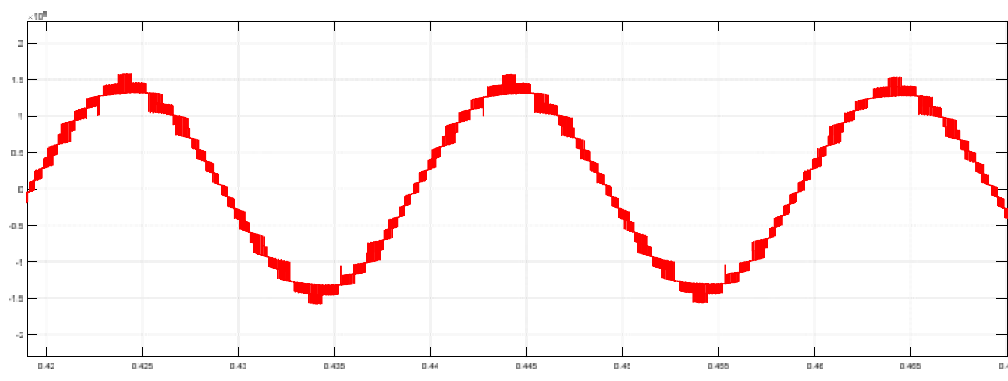


Figure 5.41 The phase to phase output voltage of 11-level MMC inverter is modulated by Carrier-shifted SPWM

The simulation results of the line-to-neutral and line-to-line voltage waveform of 15-level, 27-level, 73-level and 101-level are modulated by the Carrier-shifted SPWM methods are shown in Figure 5.43, Figure 5.44, Figure 5.45 and Figure 5.46 respectively. From simulation results that shown the output waveforms are nearly the sinusoidal waveform according the number of output voltage level.

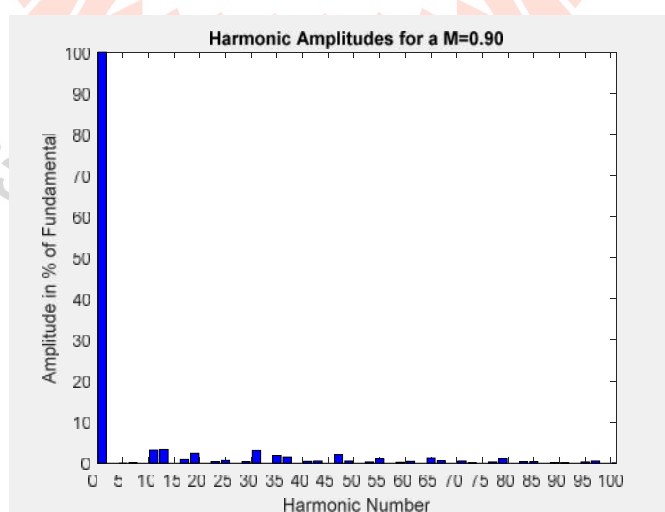


Figure 5.42 The phase to phase voltage harmonic is measured of 11-level MMC inverter is modulated by Carrier-shifted SPWM, the $THD_V = 7.3\%$

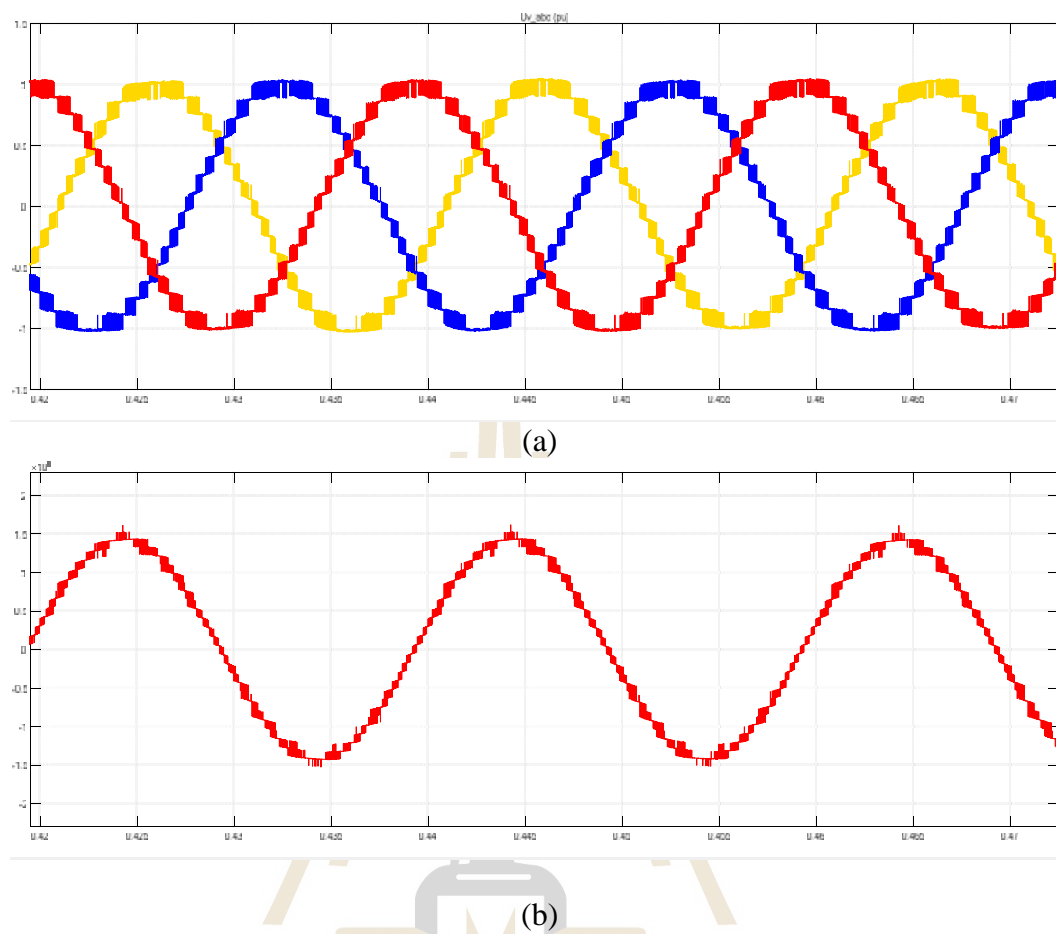
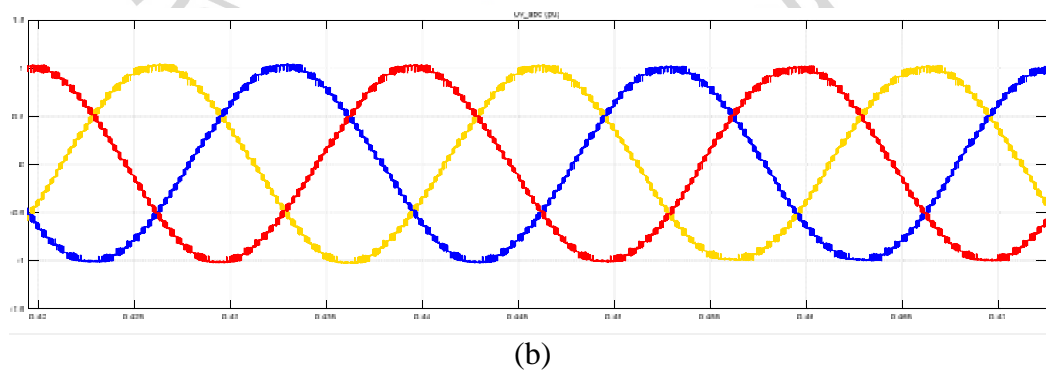


Figure 5.43 The output voltage waveform of 15-level MMC inverter is modulated by Carrier-shifted SPWM, (a) the three-phase waveforms, (b) the line-to-line waveform



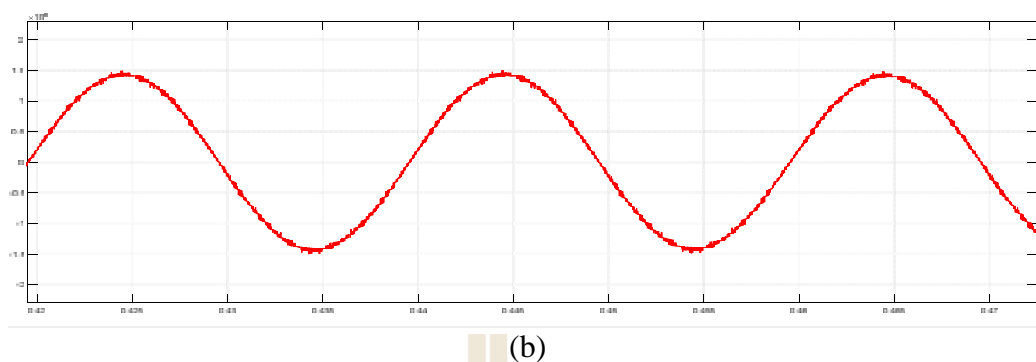


Figure 5.44 The output voltage waveform of 27-level MMC inverter is modulated by Carrier-shifted SPWM, (a) the three-phase waveforms, (b) the line-to-line waveform

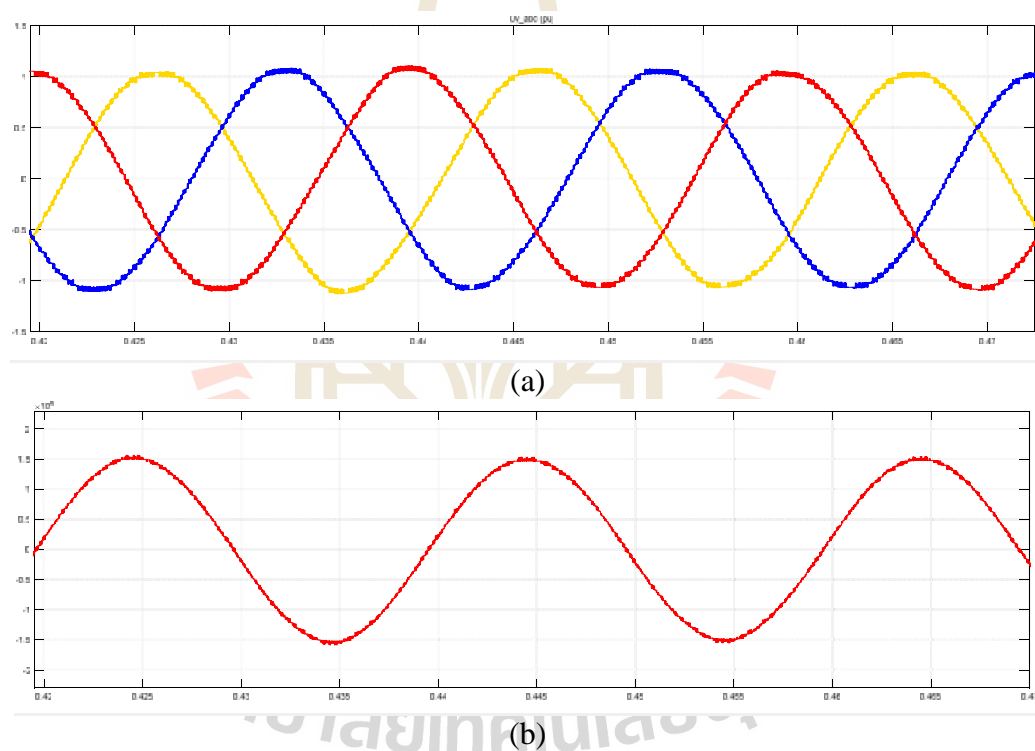


Figure 5.45 The output voltage waveform of 73-level MMC inverter is modulated by Carrier-shifted SPWM, (a) the three-phase waveforms, (b) the line-to-line waveform

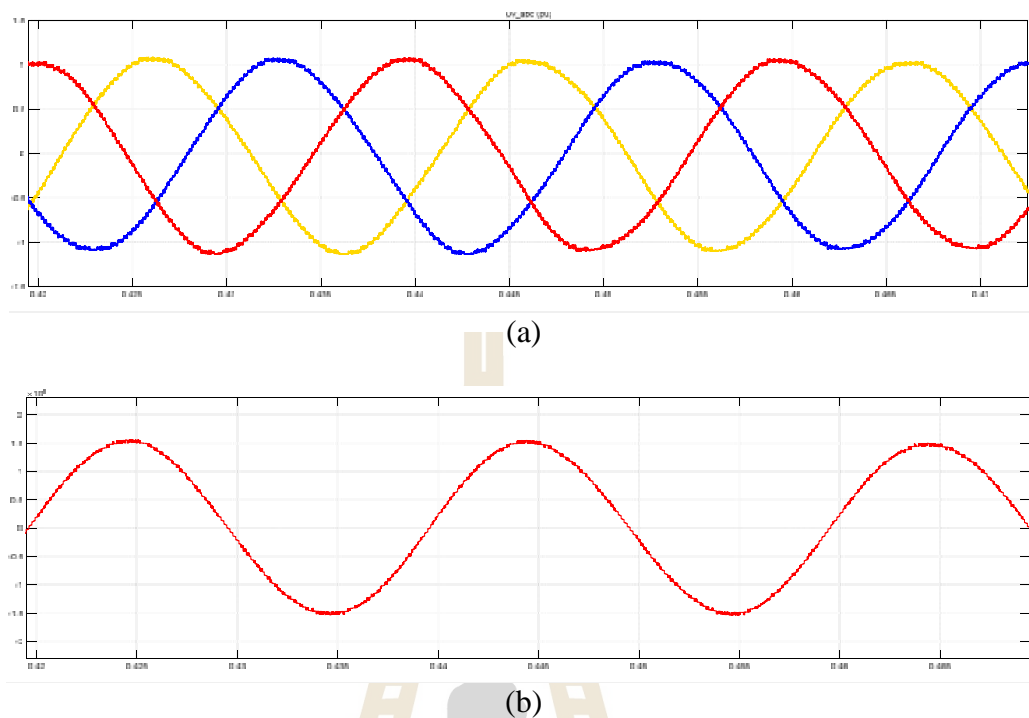


Figure 5.46 The output voltage waveform of 101-level MMC inverter is modulated by Carrier-shifted SPWM, (a) the three-phase waveforms, (b) the line-to-line waveform

The simulation results of the line-to-line voltage harmonics and THD of 15-level, 27-level, 73-level and 101-level are shown in Figure 5.47, Figure 5.48, Figure 5.49 and Figure 5.50 respectively. From simulation results that shown the individual harmonic and THD are according to the IEEE requirements.

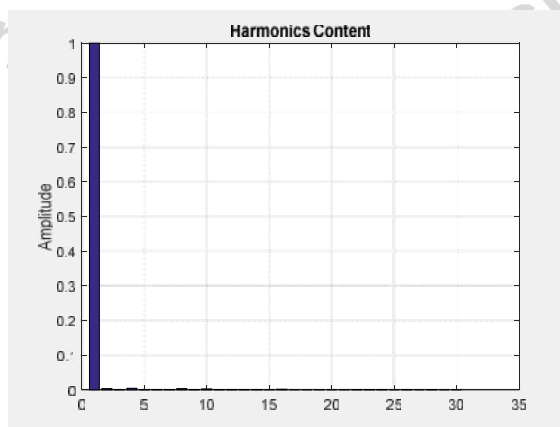


Figure 5.47 The line-to-line voltage harmonic contents of 15-level MMC inverter

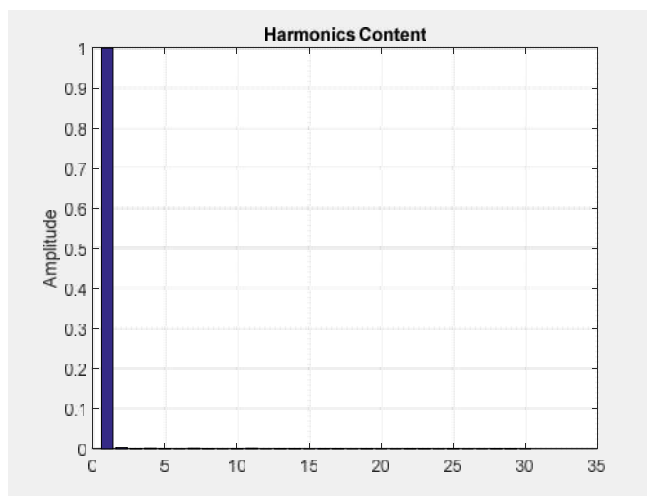


Figure 5.48 The line-to-line voltage harmonic contents of 27-level MMC inverter

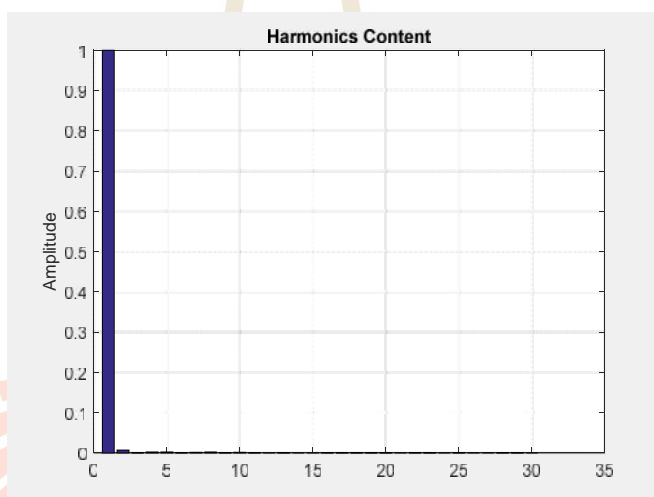


Figure 5.49 The line-to-line voltage harmonic contents of 73-level MMC inverter

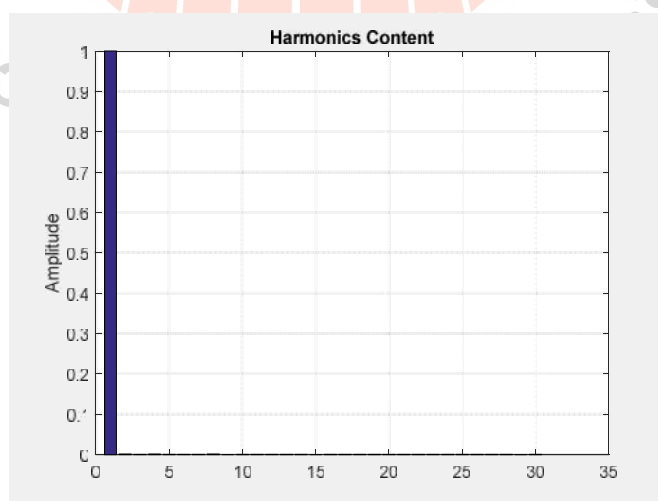


Figure 5.50 The line-to-line voltage harmonic contents of 101-level MMC inverter

The harmonic contents of line-to-line voltage of 15-level, 27-level, 73-level and 101-level are modulated by the Carrier-shifted SPWM methods are shown in Figure 5.47 to Figure 5.50. From simulation results that shown the individual harmonic content and THD of their inverters are according to the IEEE standard requirements.

For simulation results of OHSW by using PSO are presented in chapter 4, the line-to-neutral and line-to-line voltage waveform of 11-level, 15-level and 27-level MMC inverter is modulated by the OHSW method are shown in Figure 5.51, Figure 5.52 and Figure 5.53 respectively, for their harmonic contents are shown in Figure 5.54 to Figure 5.56.

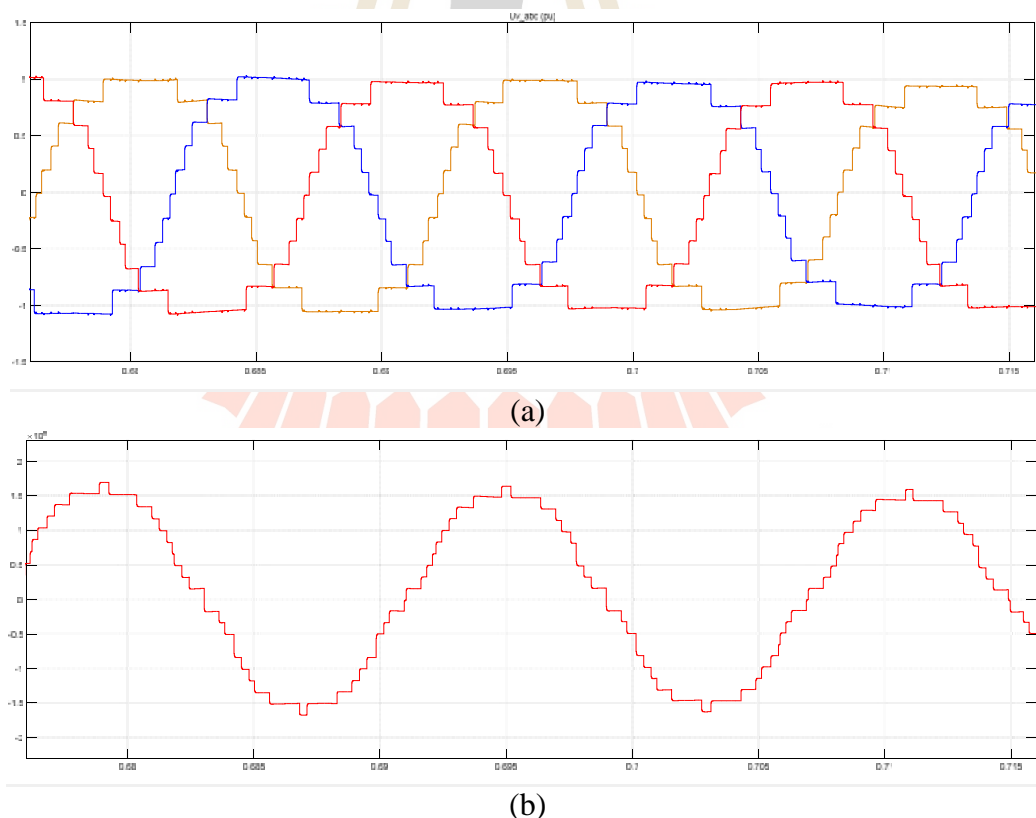
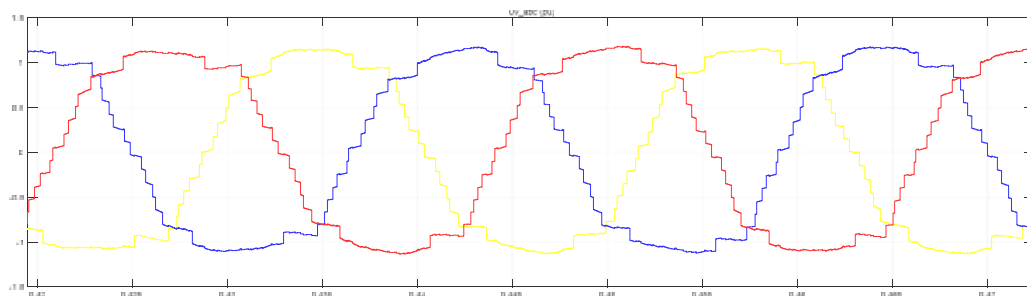
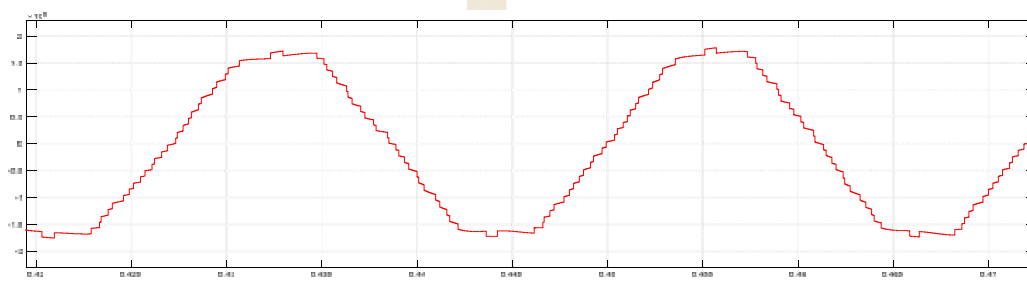


Figure 5.51 The output voltage waveform of 11-level MMC inverter is modulated by OHSW method, (a) three-phase waveforms, (b) line-to-line voltage waveform

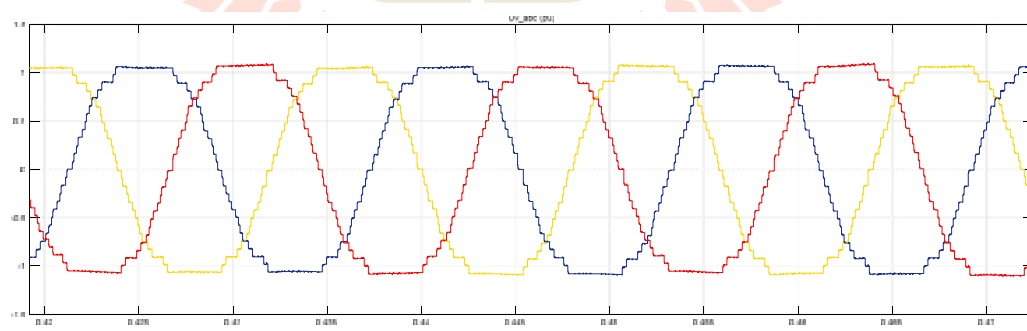


(a)



(b)

Figure 5.52 The output voltage waveform of 15-level MMC inverter is modulated by OHSW method, (a) three-phase waveforms, (b) line-to-line voltage waveform



(a)

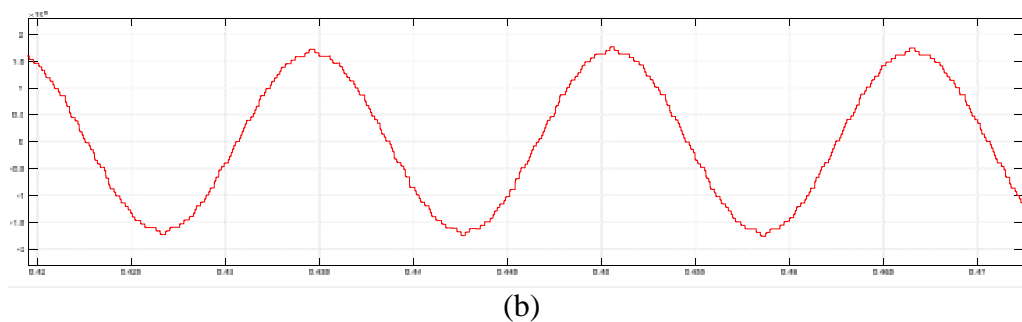


Figure 5.53 The output voltage waveform of 27-level MMC inverter is modulated by OHSW method, (a) three-phase waveforms, (b) line-to-line voltage waveform

The MMC based VSC- HVDC had generated a large number of output voltage level, this advantage it can prepared and selected the number of voltage level for optimized the number of power electronic devices and the harmonics requirement.

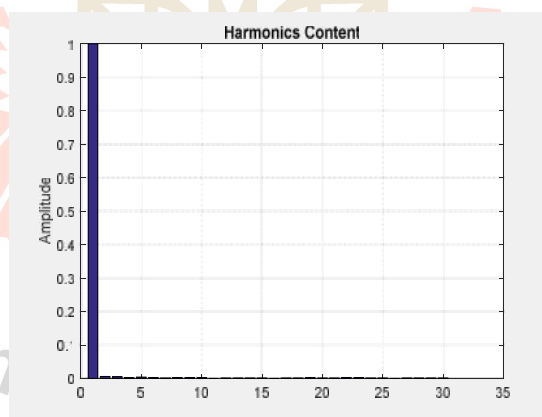


Figure 5.54 The line-to-line voltage harmonic of 11-level converter (OHSW)

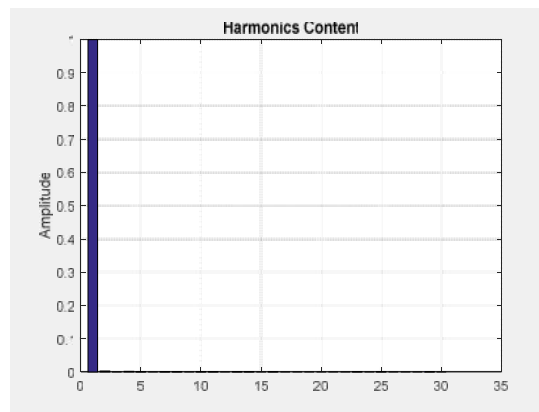


Figure 5.55 The line-to-line voltage harmonic of 15-level converter (OHSW)

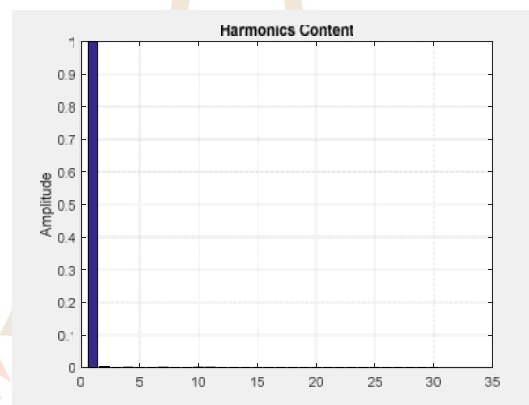


Figure 5.56 The line-to-line voltage harmonic of 27-level converter (OHSW)

Therefore, from simulation results of OHSW modulation technique are present in chapter 4 and result from the simulation in this chapter can be summarize and compare the THD in table 2. Form this table, the line-to-line voltage THD at PCC of 11-level and above according to the IEEE standard requirements and modulation by OHSW method are better than SPWM method and not required the output voltage filters.

Table 5.2 The comparison of THD of multilevel converter

Number of Level	PSO (THD %)	Inverter THD (%)		THD at PCC (%)	
		OHSW	SPWM	OHSW	SPWM
3-Level	30.26	53.63	73.20	45	61
9-Level	11.38	15.42	21.50	8.5	14.4
11-Level	8.93	7.24	7.30	1.4	2.2
15-Level	4.26	4.18	4.75	1.2	1.0
27-Level	3.16	3.20	3.35	0.7	0.9
73-Level	2.11	2.18	2.23	0.3	0.4
101-Level	1.32	1.45	1.69	0.2	0.3

5.7 Conclusions

This chapter is presented the particle swarm optimization is prepared the harmonic switching angles for modular multilevel converter application for high voltage direct current is interconnected between offshore wind farm and onshore power systems. The modeling and control are applied the vector current control that conventional used for two or three level voltage source, this paper are applied to use for modular multilevel converters. The control system attempts to decouple the reactive power and active power responses. The simulation results are shown the stability of the systems that the current are increased and after faults clearing. For performance of the modular multilevel converter, this chapter is verified by compare the line-to-line harmonics and THD output voltage on the converter bus and PCC bus. From simulation results are shown the 11-level and above converters can be achieved

to the IEEE 519-2014 standard requirements. The THD performance, all of OHSW modulation technique is better than the Carrier-shifted SPWM about 12.71% in average. The simulation results are shown the artificial intelligent particle swarm optimization can help to analysis for the selection of the method for implement.

